

Kinetic freeze-out temperatures in central and peripheral collisions: Which one is larger?

Hai-Ling Lao, Fu-Hu Liu*, Bao-Chun Li, Mai-Ying Duan

Institute of Theoretical Physics, Shanxi University, Taiyuan, Shanxi 030006, China

Abstract: The kinetic freeze-out temperatures T_0 in nucleus-nucleus collisions at the Relativistic Heavy Ion Collider (RHIC) and Large Hadron Collider (LHC) energies are extracted by four methods: i) the Blast-Wave model with Boltzmann-Gibbs statistics (the BGBW model), ii) the Blast-Wave model with Tsallis statistics (the TBW model), iii) the Tsallis distribution with flow effect (the improved Tsallis distribution), and iv) the intercept in $T = T_0 + am_0$ (the alternative method), where m_0 denotes the rest mass and T denotes the effective temperature which can be obtained by different distribution functions. It is found that the values of T_0 obtained by the four methods are incongruous in some cases. In particular, the relative sizes of T_0 in central and peripheral collisions obtained by the the first method with the traditional treatment are contradictory in tendency with others. With a new treatment for the first method, a recalculation presents a consistent result with others. The kinetic freeze-out temperature in central collisions is larger than that in peripheral collisions.

Keywords: kinetic freeze-out temperature, methods for extraction, central collisions, peripheral collisions

PACS: 25.75.Ag, 25.75.Dw, 24.10.Pa

1 Introduction

Temperature is an important concept in high energy nucleus-nucleus collisions. Usually, three types of temperatures which contain the chemical freeze-out temperature, kinetic freeze-out temperature, and effective temperature are used in literature [1–5]. The chemical freeze-out temperature describes the excitation degree of the interacting system at the stage of chemical equilibrium in which the chemical components (relative fractions) of particles are fixed. The kinetic freeze-out temperature describes the excitation degree of the interacting system at the stage of kinetic and thermal equilibrium in which the (transverse) momentum spectra of particles are no longer changed. The effective temperature is not a real temperature. In fact, the effective temperature is related to particle mass and can be extracted from the transverse momentum spectra by using some distribution laws such as the standard (Boltzmann, Fermi-Dirac, and Bose-Einstein), Tsallis, and so forth.

Generally, the chemical freeze-out temperature is usually obtained from the particle ratios [6–8]. It is

equal to or larger than the kinetic freeze-out temperature due to the the chemical equilibrium being meanwhile or earlier than the kinetic equilibrium. The effective temperature is larger than the kinetic freeze-out temperature due to mass or flow effect [9, 10]. Both the chemical and effective temperatures in central nucleus-nucleus collisions are larger than those in peripheral collisions due to more violent interactions occurring in central collisions. In fact, central collisions contain more nucleons, and peripheral collisions contains less nucleons. Usually, there are small dissents in the extractions of chemical freeze-out temperature and effective temperature. As for the extraction of kinetic freeze-out temperature, the situations are largely non-uniform.

Currently, four main methods are used in the extraction of kinetic freeze-out temperature T_0 , which are i) the Blast-Wave model with Boltzmann-Gibbs statistics (the BGBW model) [11–13], ii) the Blast-Wave model with Tsallis statistics (the TBW model) [14], iii) the Tsallis distribution with flow effect (the improved Tsallis distribution) [15, 16], and iv) the intercept in $T = T_0 + am_0$ (the alternative method) [12, 17–20], where m_0 denotes the rest mass and T denotes the ef-

*E-mail: fuhuliu@163.com; fuhuliu@sxu.edu.cn

fective temperature which can be obtained by different distribution functions. In detail, the alternative method can be divided into a few sub-methods due to different distributions being used. Generally, we are inclined to use the standard and Tsallis distributions in the alternative method due to the standard distribution being closest to the ideal gas model in thermodynamics and the Tsallis distribution describing the two- or three-component standard distribution [21].

The kinetic freeze-out temperature T_0 and the mean transverse radial flow velocity β_T can be simultaneously extracted by the first three methods. The alternative method needs further treatments for extracting the flow velocity. In our recent works [22–24], the mean transverse flow velocity β_T is regarded as the slope in the relation $\langle p_T \rangle = b_1 + \beta_T \overline{m}$, where $\langle p_T \rangle$ denotes the mean value of transverse momenta p_T , b_1 is a parameter which has no obvious meaning, and \overline{m} denotes the mean moving mass. The mean flow velocity β is regarded as the slope in the relation $\langle p \rangle = b_2 + \beta \overline{m}$, where $\langle p \rangle$ denotes the mean value of momenta p and b_2 is a parameter which has no obvious meaning. Although the mean transverse radial flow and mean transverse flow are not exactly the same, we use the same symbol to denote their velocities and neglect the difference between them. In fact, the mean transverse radial flow contains only the isotropic flow, and the mean transverse flow contains both the isotropic and anisotropic flows. The isotropic flow is mainly caused by isotropic expansion of the interacting system, and the anisotropic flow is mainly caused by anisotropic squeeze between two incoming nuclei.

We are interested in the coincidence and difference among the four methods in the extractions of T_0 and β_T . In this paper, we shall use the four methods to extract T_0 and β_T from the p_T spectra of identified particles produced in central and peripheral gold-gold (Au-Au) collisions at the center-of-mass energy per nucleon pair $\sqrt{s_{NN}} = 200$ GeV (the top RHIC energy) and in central and peripheral lead-lead (Pb-Pb) collisions at $\sqrt{s_{NN}} = 2.76$ TeV (one of the LHC energies). The modelling results on the p_T spectra are compared with the experimental data of the PHENIX [25, 26] and ALICE Collaborations [27, 28], and the modelling results on T_0 and β_T in different collisions and by different methods are compared each other.

The rest part of this paper is structured as follows.

The formalism and method are shortly described in section 2. Results and discussion are given in section 3. Finally, we summarize our main observations and conclusions in section 4.

2 The formalism and method

The four methods can be found in related references [11–20]. To give a whole representation of this paper, we present directly and concisely the four methods in the following. In the representation, some quantities such as the kinetic freeze-out temperature, the mean transverse (radial) flow velocity, and the effective temperature in different methods are uniformly denoted by T_0 , β_T , and T , respectively, though different methods correspond to different values. All of the modelling descriptions are presented at the mid-rapidity which uses the rapidity $y \approx 0$ and results in $\cosh(y) \approx 1$ which appears in some methods. At the same time, the quantum effect and chemical potential in the p_T spectra are neglected due to their small influences in high energy collisions. This means that we can give up the Fermi-Dirac and Bose-Einstein distributions, and use only the Boltzmann distribution in the case of considering the standard distribution.

According to refs. [11–13], the BGBW model results in the p_T distribution to be

$$f_1(p_T) = C_1 p_T m_T \int_0^R r dr \times I_0 \left[\frac{p_T \sinh(\rho)}{T_0} \right] K_1 \left[\frac{m_T \cosh(\rho)}{T_0} \right], \quad (1)$$

where C_1 is the normalized constant which results in $\int_0^\infty f_1(p_T) dp_T = 1$, I_0 and K_1 are the modified Bessel functions of the first and second kinds respectively, $m_T = \sqrt{p_T^2 + m_0^2}$ is the transverse mass, $\rho = \tanh^{-1}[\beta(r)]$ is the boost angle, $\beta(r) = \beta_S(r/R)^{n_0}$ is a self-similar flow profile, β_S is the flow velocity on the surface of the thermal source, r/R is the relative radial position in the thermal source, and n_0 is a free parameter which is customarily chosen to be 2 [11] due to the quadratic profile resembling the solutions of hydrodynamics closest [29]. Generally, $\beta_T = (2/R^2) \int_0^R r \beta(r) dr = 2\beta_S/(n_0+2)$. In the case of $n_0 = 2$ as used in ref. [11], we have $\beta_T = 0.5\beta_S$ [30].

According to refs. [14], the TBW model results in

the p_T distribution to be

$$f_2(p_T) = C_2 p_T m_T \int_{-\pi}^{\pi} d\phi \int_0^R r dr \left\{ 1 + \frac{q-1}{T_0} [m_T \cosh(\rho) - p_T \sinh(\rho) \cos(\phi)] \right\}^{-q/(q-1)}, \quad (2)$$

where C_2 is the normalized constant which results in $\int_0^\infty f_2(p_T) dp_T = 1$ and q is an entropy index characterizing the degree of non-equilibrium. In the case of $n_0 = 1$ as used in ref. [14], we have $\beta_T = 2\beta_S/(n_0+2) = (2/3)\beta_S$ due to the same flow profile as in the BGBW model. We would like to point out that the index $-q/(q-1)$ in Eq. (2) replaced $-1/(q-1)$ in ref. [14] due to q being very close to 1. In fact, the difference between the results corresponding to $-q/(q-1)$ and $-1/(q-1)$ are small in the Tsallis distribution [31].

According to refs. [15, 16], the improved Tsallis distribution in terms of p_T is

$$f_3(p_T) = C_3 \left\{ 2T_0[rI_0(s)K_1(r) - sI_1(s)K_0(r)] - (q-1)T_0r^2I_0(s)[K_0(r) + K_2(r)] + 4(q-1)T_0rsI_1(s)K_1(r) - (q-1)T_0s^2K_0(r)[I_0(s) + I_2(s)] + \frac{(q-1)}{4}T_0r^3I_0(s)[K_3(r) + 3K_1(r)] - \frac{3(q-1)}{2}T_0r^2s[K_2(r) + K_0(r)]I_1(s) + \frac{3(q-1)}{2}T_0s^2r[I_0(s) + I_2(s)]K_1(r) - \frac{(q-1)}{4}T_0s^3[I_3(s) + 3I_1(s)]K_0(r) \right\}, \quad (3)$$

where C_3 is the normalized constant which results in $\int_0^\infty f_3(p_T) dp_T = 1$, $r \equiv \gamma m_T/T_0$, $s \equiv \gamma \beta_T p_T/T_0$, $\gamma = 1/\sqrt{1-\beta_T^2}$, and $I_{0-3}(s)$ and $K_{0-3}(r)$ are the modified Bessel functions of the first and second kinds respectively.

As for the alternative method [12, 17–20, 22–24], to use the relations $T = T_0 + am_0$, $\langle p_T \rangle = b_1 + \beta_T \overline{m}$, and $\langle p \rangle = b_2 + \beta \overline{m}$, we can choose the standard and Tsallis distributions to fit the p_T spectra of identified particles produced in high energy collisions. Because we give up the Fermi-Dirac and Bose-Einstein distributions, only the Boltzmann distribution is used in the case of considering the standard distribution in the present work. Both the Boltzmann and Tsallis distributions have more

than one forms. We choose the form of Boltzmann distribution [32]

$$f_{4a}(p_T) = C_{4a} p_T m_T \exp\left(-\frac{m_T}{T}\right) \quad (4)$$

and the form of Tsallis distribution [31, 32]

$$f_{4b}(p_T) = C_{4b} p_T m_T \left(1 + \frac{q-1}{T} m_T\right)^{-q/(q-1)}, \quad (5)$$

where C_{4a} and C_{4b} are the normalized constants which result in $\int_0^\infty f_{4a}(p_T) dp_T = 1$ and $\int_0^\infty f_{4b}(p_T) dp_T = 1$ respectively.

It should be noticed that the above five distributions are only valid for the spectra in a narrow p_T range. That is, they describe only the soft excitation process. Even if for the soft process, the Boltzmann distribution is not enough to fit the p_T spectra in some cases. In fact, two- or three-component Boltzmann distribution have to be used, in which T is the average weighted the effective temperatures obtained from different components. We have

$$f_{4a}(p_T) = \sum_{i=1}^m k_i C_{4ai} p_T m_T \exp\left(-\frac{m_T}{T_i}\right) \quad (6)$$

and

$$T = \sum_{i=1}^m k_i T_i, \quad (7)$$

where $m = 2$ or 3 denotes the number of components, and k_i , C_{4ai} , and T_i denote the contribution ratio (relative contribution or fraction), normalization constant, and effective temperature related to the i -th component, respectively.

For the spectra in a wide p_T range, we have to consider the contribution of hard scattering process. Generally, the contribution of hard process is parameterized to an inverse power-law

$$f_H(p_T) = A p_T \left(1 + \frac{p_T}{p_0}\right)^{-n} \quad (8)$$

which is resulted from the QCD (quantum chromodynamics) calculus [33–35], where p_0 and n are free parameters, and A is the normalized constant which depends on p_0 and n and results in $\int_0^\infty f_H(p_T) dp_T = 1$.

To describe the spectra in a wide p_T range, we can use a superposition of both contributions of soft and hard processes. The contribution of soft process is described by one of the BGBW model, the TBW model,

the improved Tsallis distribution, the Boltzmann distribution or two- or three-component Boltzmann distribution, and the Tsallis distribution, while the contribution of hard process is described by the inverse power-law. We have the superposition

$$f_0(p_T) = kf_S(p_T) + (1 - k)f_H(p_T), \quad (9)$$

where k denotes the contribution ratio of the soft process and results naturally in $\int_0^\infty f_0(p_T)dp_T = 1$, and $f_S(p_T)$ denotes one of the five distributions discussed in the four methods.

3 Results and discussion

Figure 1 presents the transverse momentum spectra, $(2\pi p_T)^{-1}d^2N/(dydp_T)$, of (a)-(c) positive charged pions (π^+), positive charged kaons (K^+), and protons (p), as well as (b)-(d) negative charged pions (π^-), negative charged kaons (K^-), and antiprotons (\bar{p}) produced in (a)-(b) 0–5% and (c)-(d) 80–92% Au-Au collisions at $\sqrt{s_{NN}} = 200$ GeV, where the spectra for different particles are multiplied by different amounts shown in the panels for the clarity. The symbols represent the experimental data of the PHENIX Collaboration measured in the rapidity range $|y| < 0.5$ [26]. The solid, dashed, dotted, dashed-dotted, and dashed-dotted-dotted curves are our results calculated by using the superpositions of i) the BGBW model (Eq. (1)) and inverse power-law (Eq. (8)), ii) the TBW model (Eq. (2)) and inverse power-law, iii) the improved Tsallis distribution (Eq. (3)) and inverse power-law, iv)_a the Boltzmann distribution (Eq. (4)) and inverse power-law, as well as iv)_b the Tsallis distribution (Eq. (5)) and inverse power-law, respectively. These different superpositions are also different methods for fitting the data. The values of free parameters T_0 , β_T , k , p_0 , and n , normalization constant N_0 which is used to fit the data, and χ^2 per degree of freedom (χ^2/dof) corresponding to the fit of method i) are listed in Table 1; the values of T_0 , q , β_T , k , p_0 , n , N_0 , and χ^2/dof corresponding to the methods ii) and iii) are listed in Tables 2 and 3 respectively; the values of T , k , p_0 , n , N_0 , and χ^2/dof corresponding to the methods iv)_a are listed in Table 4; and the values of T , q , k , p_0 , n , N_0 , and χ^2/dof corresponding to the methods iv)_b are listed in Table 5. One can see that, in most cases, all of the considered methods describe the p_T spectra

of identified particles produced in central (0–5%) and peripheral (80–92%) Au-Au collisions at $\sqrt{s_{NN}} = 200$ GeV.

Figure 2 is the same as Figure 1, but it shows the spectra, $(1/N_{EV})(2\pi p_T)^{-1}d^2N/(dydp_T)$, in (a)-(b) 0–5% and (c)-(d) 80–90% Pb-Pb collisions at $\sqrt{s_{NN}} = 2.76$ TeV, where N_{EV} on the vertical axis denotes the number of events, which is usually omitted. The experimental data of the ALICE Collaboration are taken from ref. [28]. One can see that, in most cases, all of the considered methods describe the p_T spectra of identified particles produced in central (0–5%) and peripheral (80–90%) Pb-Pb collisions at $\sqrt{s_{NN}} = 2.76$ TeV.

Based on the descriptions of p_T spectra, the first three methods can give T_0 and β_T conveniently, though the values of parameters are possibly inharmonious due to different methods. In particular, the value of T_0 obtained by the method i) in peripheral collisions is greater than that in central collisions, which is different from the methods ii) and iii) which obtain an opposite result. According to the traditional treatment in refs. [11, 14], the values of β_T obtained by the methods i) and ii) in peripheral collisions are taken to be nearly zero, which are different from the method iii) which obtains a value of about $0.6c$ in both central and peripheral collisions.

To obtain the values of T_0 , β_T , and β by the methods iv)_a and iv)_b, we analyze the values of T presented in Tables 4 and 5, and calculate $\langle p_T \rangle$, $\langle p \rangle$, and \bar{m} based on the values of parameters listed in Tables 4 and 5. In the calculations performed from p_T to $\langle p \rangle$ and \bar{m} by the Monte Carlo method, an isotropic assumption in the rest frame of emission source is used [22–24].

The relations between T and m_0 , $\langle p_T \rangle$ and \bar{m} , as well as $\langle p \rangle$ and \bar{m} are shown in Figures 3, 4, and 5, respectively, where panels (a) and (b) correspond to the methods iv)_a and iv)_b which use the Boltzmann and Tsallis distributions respectively. The symbols in Figure 3 represent values of T listed in Tables 4 and 5 for different m_0 . The symbols in Figures 4 and 5 represent values of $\langle p_T \rangle$ and $\langle p \rangle$ for different \bar{m} respectively, which are calculated due to the parameters listed in Tables 4 and 5 and the isotropic assumption in the rest frame of emission source. The solid and dashed lines in the three figures are the results fitted by the method of least squares for the positive and negative charged particles respectively. The values of intercepts, slopes,

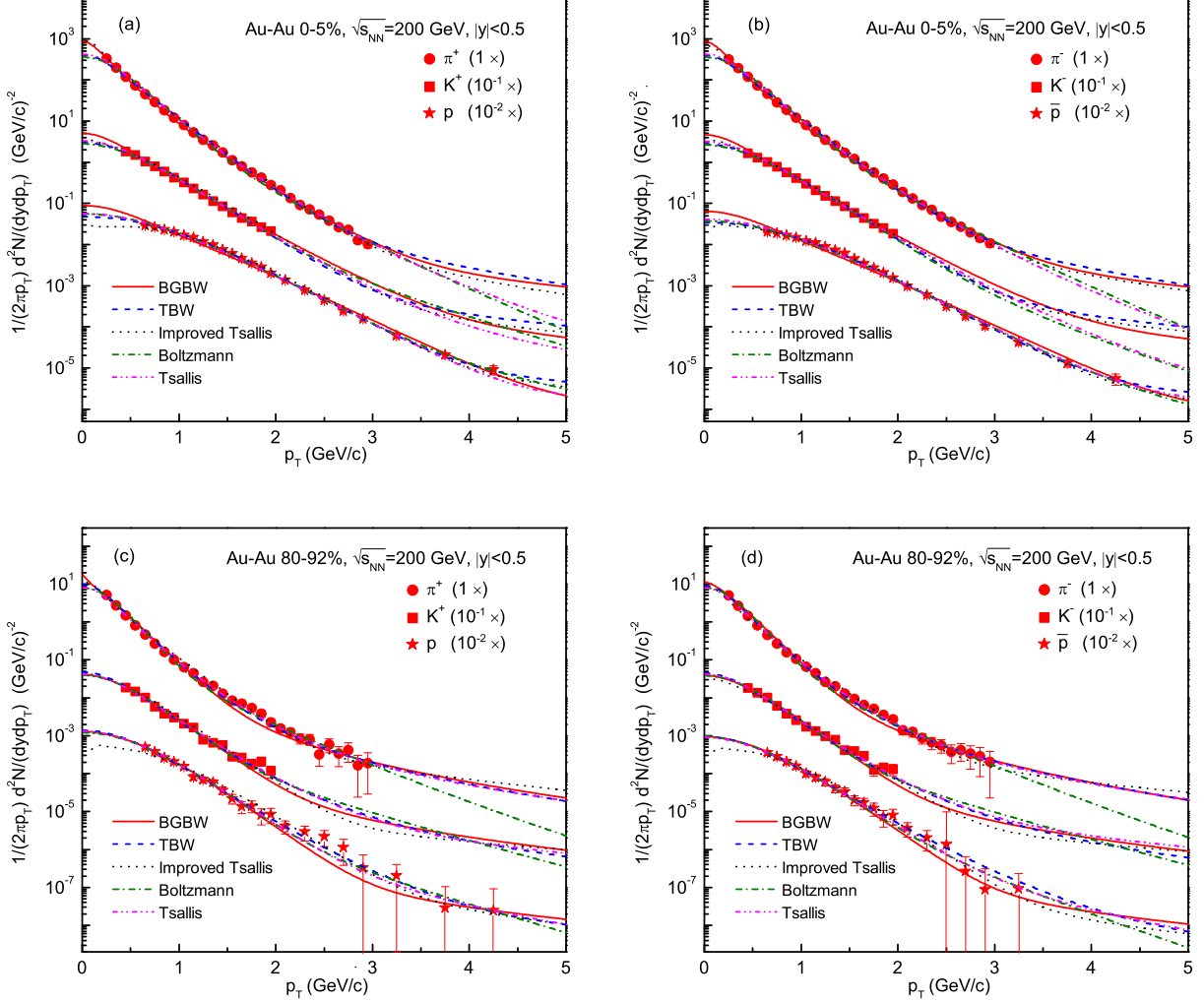


Fig. 1. Transverse momentum spectra of (a)-(c) π^+ , K^+ , and p , as well as (b)-(d) π^- , K^- , and \bar{p} produced in (a)-(b) 0–5% and (c)-(d) 80–92% Au-Au collisions at $\sqrt{s_{NN}} = 200$ GeV, where the spectra for different particles are multiplied by different amounts shown in the panels for the clarity. The symbols represent the experimental data of the PHENIX Collaboration measured in the rapidity range $|y| < 0.5$ [26]. The solid, dashed, dotted, dashed-dotted, and dashed-dotted-dotted curves are our results calculated by using the superpositions of the BGBW model (Eq. (1)) and inverse power-law (Eq. (8)), the TBW model (Eq. (2)) and inverse power-law, the improved Tsallis distribution (Eq. (3)) and inverse power-law, the Boltzmann distribution (Eq. (4)) and inverse power-law, as well as the Tsallis distribution (Eq. (5)) and inverse power-law, respectively.

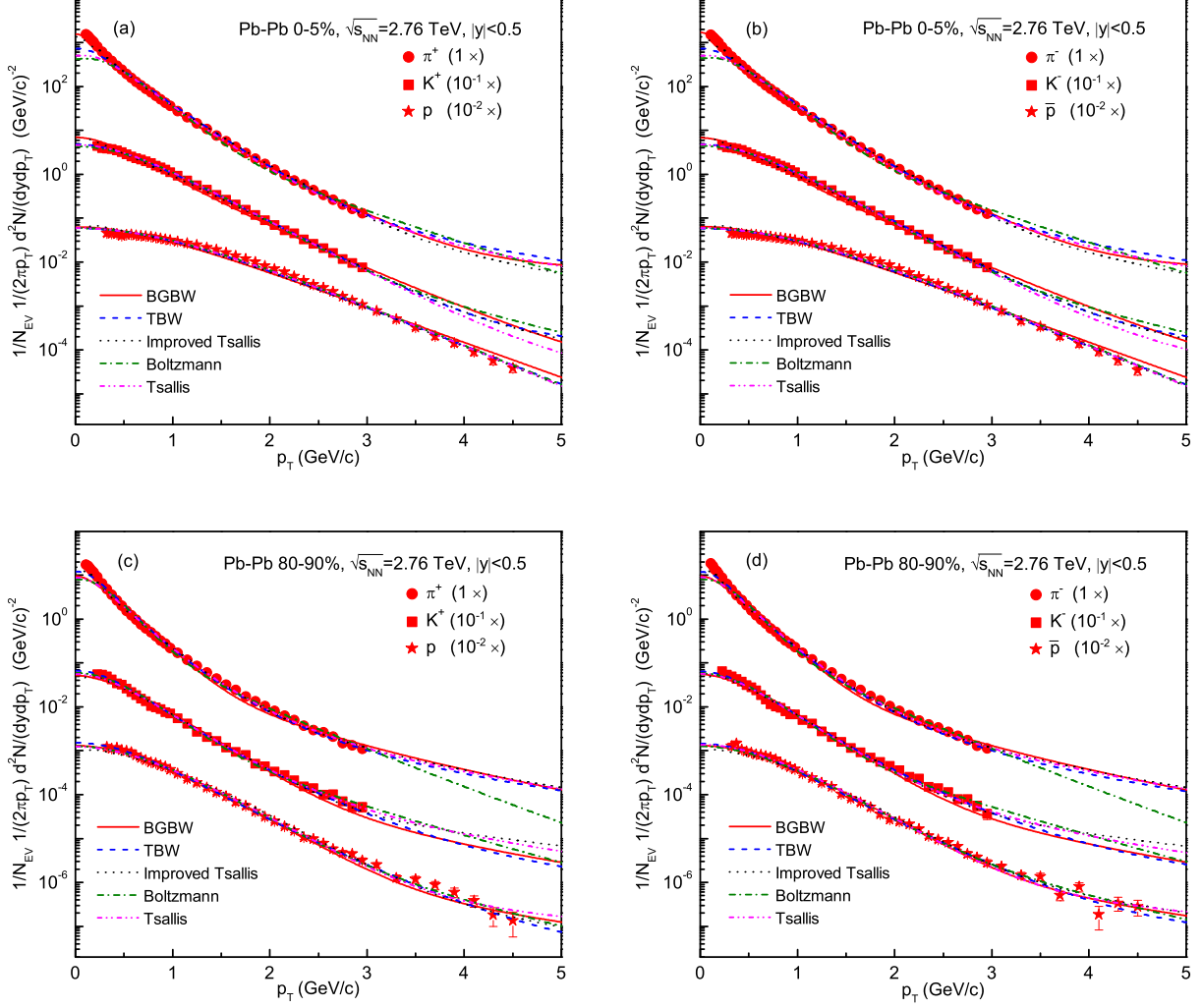


Fig. 2. Same as Figure 1, but showing the spectra in (a)-(b) 0–5% and (c)-(d) 80–90% Pb-Pb collisions at $\sqrt{s_{NN}} = 2.76$ TeV, where N_{EV} on the vertical axis denotes the number of events, which is usually omitted. The experimental data of the ALICE Collaboration are taken from ref. [28].

Table 1. Values of free parameters (T_0 , β_T , k , p_0 , and n), normalization constant (N_0), and χ^2/dof corresponding to the fits of the BGBW model and inverse power-law in Figures 1 and 2, where $n_0 = 2$ in the self-similar flow profile is used as ref. [11].

Fig.	Cent.	Part.	T_0 (GeV)	β_T (c)	k	p_0 (GeV/c)	n	N_0	χ^2/dof
1(a)	0-5%	π^+	0.109 ± 0.003	0.412 ± 0.005	0.998 ± 0.002	1.109 ± 0.036	3.297 ± 0.095	218.885 ± 16.553	0.834
		K^+	0.123 ± 0.004	0.408 ± 0.006	0.996 ± 0.004	3.809 ± 0.115	4.597 ± 0.125	22.475 ± 1.365	9.501
		p	0.127 ± 0.004	0.399 ± 0.005	0.998 ± 0.002	6.175 ± 0.232	3.865 ± 0.116	5.985 ± 0.312	19.755
1(b)	0-5%	π^-	0.109 ± 0.003	0.412 ± 0.005	0.998 ± 0.002	1.109 ± 0.036	3.297 ± 0.095	219.465 ± 16.558	0.866
		K^-	0.123 ± 0.004	0.408 ± 0.006	0.996 ± 0.004	3.809 ± 0.115	4.597 ± 0.125	21.595 ± 1.345	15.355
		\bar{p}	0.128 ± 0.004	0.401 ± 0.005	0.998 ± 0.002	6.175 ± 0.232	3.865 ± 0.116	4.344 ± 0.212	25.259
1(c)	80-92%	π^+	0.159 ± 0.004	$0.000^{+0.016}_{-0}$	0.822 ± 0.012	0.309 ± 0.012	4.597 ± 0.215	3.175 ± 0.121	3.155
		K^+	0.203 ± 0.005	$0.000^{+0.016}_{-0}$	0.955 ± 0.009	0.939 ± 0.016	4.297 ± 0.197	0.197 ± 0.010	3.678
		p	0.205 ± 0.005	$0.000^{+0.016}_{-0}$	0.985 ± 0.009	0.489 ± 0.023	3.597 ± 0.155	0.078 ± 0.004	0.945
1(d)	80-92%	π^-	0.153 ± 0.004	$0.000^{+0.016}_{-0}$	0.905 ± 0.011	0.741 ± 0.013	5.587 ± 0.226	3.005 ± 0.106	3.595
		K^-	0.203 ± 0.005	$0.000^{+0.016}_{-0}$	0.955 ± 0.009	0.939 ± 0.016	4.297 ± 0.195	0.186 ± 0.009	1.839
		\bar{p}	0.208 ± 0.005	$0.000^{+0.016}_{-0}$	0.985 ± 0.009	0.489 ± 0.023	3.597 ± 0.155	0.058 ± 0.003	0.454
2(a)	0-5%	π^+	0.124 ± 0.003	0.438 ± 0.006	0.997 ± 0.003	1.909 ± 0.086	1.097 ± 0.081	448.385 ± 28.556	1.394
		K^+	0.184 ± 0.003	0.395 ± 0.005	0.998 ± 0.002	1.809 ± 0.085	3.597 ± 0.113	39.375 ± 2.255	4.608
		p	0.445 ± 0.005	0.145 ± 0.006	0.995 ± 0.005	4.309 ± 0.136	8.297 ± 0.165	6.585 ± 0.226	6.731
2(b)	0-5%	π^-	0.122 ± 0.003	0.438 ± 0.006	0.997 ± 0.003	1.909 ± 0.086	1.097 ± 0.081	482.565 ± 35.152	1.339
		K^-	0.182 ± 0.003	0.399 ± 0.005	0.998 ± 0.002	1.809 ± 0.085	3.597 ± 0.113	38.455 ± 2.255	3.648
		\bar{p}	0.445 ± 0.005	0.144 ± 0.006	0.998 ± 0.002	5.719 ± 0.165	8.565 ± 0.165	6.724 ± 0.232	4.813
2(c)	80-90%	π^+	0.183 ± 0.004	$0.000^{+0.017}_{-0}$	0.900 ± 0.009	2.409 ± 0.089	7.347 ± 0.133	3.185 ± 0.185	12.659
		K^+	0.268 ± 0.004	$0.000^{+0.017}_{-0}$	0.915 ± 0.009	2.031 ± 0.085	6.097 ± 0.165	0.300 ± 0.012	3.049
		p	0.298 ± 0.004	$0.000^{+0.017}_{-0}$	0.975 ± 0.009	6.909 ± 0.225	8.997 ± 0.161	0.102 ± 0.006	1.505
2(d)	80-90%	π^-	0.183 ± 0.004	$0.000^{+0.017}_{-0}$	0.900 ± 0.009	2.409 ± 0.249	7.347 ± 0.323	3.185 ± 0.185	12.254
		K^-	0.260 ± 0.004	$0.000^{+0.017}_{-0}$	0.895 ± 0.010	2.031 ± 0.085	6.097 ± 0.165	0.311 ± 0.009	3.072
		\bar{p}	0.297 ± 0.004	$0.000^{+0.017}_{-0}$	0.965 ± 0.013	6.909 ± 0.225	8.997 ± 0.161	0.102 ± 0.006	1.308

Table 2. Values of free parameters (T_0 , q , β_T , k , p_0 , and n), normalization constant (N_0), and χ^2/dof corresponding to the fits of the TBW model and inverse power-law in Figures 1 and 2, where $n_0 = 1$ is used as ref. [14].

Fig.	Cent.	Part.	T_0 (GeV)	q	β_T (c)	k	p_0 (GeV/c)	n	N_0	χ^2/dof
1(a)	0-5%	π^+	0.104 ± 0.003	1.008 ± 0.005	0.469 ± 0.010	0.993 ± 0.003	2.597 ± 0.095	6.409 ± 0.132	149.852 ± 11.235	1.390
		K^+	0.113 ± 0.004	1.008 ± 0.005	0.469 ± 0.010	0.990 ± 0.006	3.597 ± 0.109	4.609 ± 0.115	17.552 ± 1.128	9.823
		p	0.119 ± 0.004	1.009 ± 0.005	0.469 ± 0.008	0.992 ± 0.002	4.437 ± 0.113	3.809 ± 0.102	4.426 ± 0.226	2.029
1(b)	0-5%	π^-	0.104 ± 0.003	1.008 ± 0.005	0.469 ± 0.010	0.994 ± 0.003	2.597 ± 0.095	6.409 ± 0.132	144.352 ± 11.119	0.964
		K^-	0.113 ± 0.004	1.008 ± 0.005	0.469 ± 0.010	0.990 ± 0.006	3.597 ± 0.109	4.609 ± 0.115	16.352 ± 1.116	4.261
		\bar{p}	0.120 ± 0.004	1.009 ± 0.005	0.469 ± 0.008	0.994 ± 0.003	4.437 ± 0.113	3.809 ± 0.102	3.202 ± 0.203	4.324
1(c)	80-92%	π^+	0.099 ± 0.003	1.073 ± 0.005	$0.000^{+0.036}_{-0}$	0.986 ± 0.004	2.397 ± 0.095	6.909 ± 0.185	2.852 ± 0.168	1.539
		K^+	0.108 ± 0.003	1.088 ± 0.005	$0.000^{+0.036}_{-0}$	0.985 ± 0.006	2.031 ± 0.085	5.058 ± 0.136	0.212 ± 0.018	2.080
		p	0.108 ± 0.004	1.068 ± 0.005	$0.000^{+0.036}_{-0}$	0.998 ± 0.001	2.051 ± 0.088	3.658 ± 0.126	0.081 ± 0.006	0.501
1(d)	80-92%	π^-	0.099 ± 0.003	1.076 ± 0.005	$0.000^{+0.036}_{-0}$	0.984 ± 0.004	2.397 ± 0.095	6.909 ± 0.185	2.652 ± 0.163	0.963
		K^-	0.108 ± 0.003	1.088 ± 0.005	$0.000^{+0.036}_{-0}$	0.985 ± 0.006	2.031 ± 0.085	5.058 ± 0.136	0.198 ± 0.016	1.054
		\bar{p}	0.108 ± 0.004	1.065 ± 0.005	$0.000^{+0.036}_{-0}$	0.998 ± 0.001	1.451 ± 0.066	3.658 ± 0.126	0.057 ± 0.006	0.265
2(a)	0-5%	π^+	0.109 ± 0.004	1.006 ± 0.003	0.525 ± 0.009	0.980 ± 0.007	3.097 ± 0.106	6.409 ± 0.122	311.042 ± 30.121	6.801
		K^+	0.145 ± 0.005	1.002 ± 0.001	0.500 ± 0.009	0.994 ± 0.004	4.097 ± 0.116	4.455 ± 0.119	34.152 ± 3.442	0.098
		p	0.178 ± 0.005	1.002 ± 0.001	0.500 ± 0.008	0.999 ± 0.001	4.546 ± 0.118	4.665 ± 0.113	6.652 ± 0.195	3.617
2(b)	0-5%	π^-	0.109 ± 0.004	1.006 ± 0.003	0.525 ± 0.009	0.980 ± 0.007	3.097 ± 0.106	6.409 ± 0.122	311.352 ± 30.521	6.686
		K^-	0.145 ± 0.005	1.002 ± 0.002	0.500 ± 0.009	0.994 ± 0.004	4.097 ± 0.116	4.455 ± 0.119	34.092 ± 3.442	0.188
		\bar{p}	0.178 ± 0.005	1.002 ± 0.001	0.500 ± 0.008	0.999 ± 0.001	4.546 ± 0.118	4.665 ± 0.113	6.552 ± 0.191	2.855
2(c)	80-90%	π^+	0.102 ± 0.004	1.108 ± 0.005	$0.000^{+0.018}_{-0}$	0.986 ± 0.005	4.385 ± 0.115	6.859 ± 0.132	3.912 ± 0.141	7.329
		K^+	0.139 ± 0.005	1.099 ± 0.005	$0.000^{+0.018}_{-0}$	0.993 ± 0.004	3.031 ± 0.098	4.058 ± 0.104	0.352 ± 0.025	1.277
		p	0.163 ± 0.005	1.076 ± 0.005	$0.000^{+0.018}_{-0}$	0.998 ± 0.002	7.251 ± 0.124	3.658 ± 0.095	0.111 ± 0.009	0.536
2(d)	80-90%	π^-	0.102 ± 0.004	1.108 ± 0.005	$0.000^{+0.018}_{-0}$	0.986 ± 0.005	4.385 ± 0.125	6.859 ± 0.112	3.841 ± 0.152	6.992
		K^-	0.141 ± 0.005	1.099 ± 0.005	$0.000^{+0.018}_{-0}$	0.992 ± 0.004	3.031 ± 0.098	4.058 ± 0.104	0.341 ± 0.025	1.551
		\bar{p}	0.165 ± 0.005	1.076 ± 0.005	$0.000^{+0.018}_{-0}$	0.994 ± 0.004	4.251 ± 0.085	1.658 ± 0.075	0.106 ± 0.009	0.715

Table 3. Values of free parameters (T_0 , q , β_T , k , p_0 , and n), normalization constant (N_0), and χ^2/dof corresponding to the fits of the improved Tsallis distribution and inverse power-law in Figures 1 and 2.

Fig.	Cent.	Part.	T_0 (GeV)	q	β_T (c)	k	p_0 (GeV/c)	n	N_0	χ^2/dof	
1(a)	0-5%	π^+	0.109 ± 0.006	1.023 ± 0.016	0.634 ± 0.019	0.991 ± 0.008	0.709 ± 0.165	4.597 ± 0.645	224.148 ± 44.212	2.205	
		K^+	0.113 ± 0.011	1.052 ± 0.037	0.634 ± 0.029	0.992 ± 0.007	2.594 ± 0.323	4.291 ± 0.935	16.743 ± 2.746	0.916	
		p	0.121 ± 0.009	1.097 ± 0.055	0.634 ± 0.021	0.991 ± 0.007	3.697 ± 0.442	4.036 ± 0.834	3.191 ± 0.477		0.940
1(b)	0-5%	π^-	0.111 ± 0.006	1.062 ± 0.025	0.590 ± 0.032	0.994 ± 0.005	0.956 ± 0.218	4.436 ± 0.585	180.622 ± 38.234	1.529	
		K^-	0.121 ± 0.011	1.067 ± 0.049	0.590 ± 0.031	0.991 ± 0.004	2.667 ± 0.331	4.286 ± 0.635	15.977 ± 4.268	1.087	
		\bar{p}	0.133 ± 0.009	1.095 ± 0.065	0.590 ± 0.028	0.992 ± 0.007	3.132 ± 0.921	4.969 ± 0.812	2.777 ± 0.564		0.971
1(c)	80-92%	π^+	0.106 ± 0.009	1.028 ± 0.017	0.572 ± 0.026	0.994 ± 0.005	2.321 ± 0.461	4.382 ± 1.454	2.731 ± 0.449	3.616	
		K^+	0.106 ± 0.008	1.028 ± 0.021	0.572 ± 0.055	0.991 ± 0.008	3.802 ± 0.395	4.161 ± 1.115	0.175 ± 0.032		1.847
		p	0.119 ± 0.009	1.013 ± 0.010	0.528 ± 0.035	0.992 ± 0.005	1.914 ± 0.258	4.945 ± 0.612	0.041 ± 0.003		1.551
1(d)	80-92%	π^-	0.115 ± 0.007	1.015 ± 0.012	0.587 ± 0.039	0.995 ± 0.004	3.419 ± 0.423	4.706 ± 0.612	2.161 ± 0.323	0.319	
		K^-	0.115 ± 0.009	1.013 ± 0.011	0.587 ± 0.039	0.990 ± 0.006	3.922 ± 0.458	4.135 ± 0.995	0.137 ± 0.022		3.075
		\bar{p}	0.116 ± 0.009	1.005 ± 0.004	0.529 ± 0.038	0.995 ± 0.004	1.859 ± 0.423	4.796 ± 0.825	0.035 ± 0.005		0.523
2(a)	0-5%	π^+	0.152 ± 0.004	1.011 ± 0.004	0.609 ± 0.013	0.985 ± 0.007	2.325 ± 0.117	6.238 ± 0.323	401.818 ± 25.552	2.115	
		K^+	0.158 ± 0.004	1.059 ± 0.008	0.609 ± 0.013	0.987 ± 0.006	2.972 ± 0.142	5.742 ± 0.285	31.282 ± 2.765	4.403	
		p	0.194 ± 0.005	1.069 ± 0.011	0.609 ± 0.013	0.991 ± 0.006	2.423 ± 0.131	6.949 ± 0.288	6.082 ± 0.458		5.460
2(b)	0-5%	π^-	0.152 ± 0.004	1.011 ± 0.004	0.609 ± 0.013	0.985 ± 0.007	2.325 ± 0.117	6.238 ± 0.323	401.818 ± 25.552	1.850	
		K^-	0.158 ± 0.004	1.059 ± 0.008	0.609 ± 0.013	0.987 ± 0.006	2.972 ± 0.142	5.742 ± 0.285	31.495 ± 2.769	0.979	
		\bar{p}	0.194 ± 0.005	1.069 ± 0.011	0.609 ± 0.013	0.993 ± 0.004	2.423 ± 0.131	6.949 ± 0.288	6.082 ± 0.458		4.115
2(c)	80-90%	π^+	0.118 ± 0.005	1.008 ± 0.005	0.625 ± 0.014	0.945 ± 0.009	2.106 ± 0.115	6.079 ± 0.295	3.718 ± 0.228	4.144	
		K^+	0.143 ± 0.004	1.011 ± 0.005	0.602 ± 0.012	0.955 ± 0.009	3.642 ± 0.121	5.122 ± 0.225	0.272 ± 0.018		1.743
		p	0.163 ± 0.005	1.007 ± 0.003	0.548 ± 0.009	0.965 ± 0.009	3.499 ± 0.121	7.059 ± 0.232	0.079 ± 0.004		2.392
2(d)	80-90%	π^-	0.118 ± 0.005	1.008 ± 0.005	0.625 ± 0.014	0.945 ± 0.009	2.106 ± 0.115	6.079 ± 0.295	3.718 ± 0.228	3.998	
		K^-	0.141 ± 0.004	1.010 ± 0.004	0.602 ± 0.012	0.955 ± 0.009	3.642 ± 0.121	5.122 ± 0.225	0.270 ± 0.016		2.413
		\bar{p}	0.155 ± 0.005	1.007 ± 0.003	0.548 ± 0.011	0.955 ± 0.009	4.699 ± 0.125	7.059 ± 0.232	0.078 ± 0.004		2.282

Table 4. Values of free parameters (T , k , p_0 , and n), normalization constant (N_0), and χ^2/dof corresponding to the fits of the Boltzmann distribution and inverse power-law in Figures 1 and 2.

Fig.	Cent.	Part.	T (GeV)	k	p_0 (GeV/c)	n	N_0	χ^2/dof
1(a)	0-5%	π^+	0.156 ± 0.004	0.813 ± 0.011	9.632 ± 0.328	33.232 ± 0.665	147.352 ± 11.232	2.199
		K^+	0.221 ± 0.004	0.901 ± 0.009	19.495 ± 1.112	39.232 ± 1.365	16.739 ± 1.115	8.210
		p	0.291 ± 0.005	0.975 ± 0.007	30.862 ± 1.165	39.258 ± 1.632	4.746 ± 0.153	4.368
1(b)	0-5%	π^-	0.156 ± 0.004	0.819 ± 0.011	10.532 ± 0.356	35.232 ± 0.585	147.352 ± 9.565	1.769
		K^-	0.225 ± 0.003	0.905 ± 0.009	15.595 ± 0.685	38.332 ± 0.986	15.702 ± 1.012	6.207
		\bar{p}	0.299 ± 0.005	0.975 ± 0.009	26.432 ± 0.896	39.232 ± 1.775	3.252 ± 0.135	6.953
1(c)	80-92%	π^+	0.122 ± 0.004	0.900 ± 0.011	8.772 ± 0.556	27.332 ± 0.898	2.752 ± 0.166	1.951
		K^+	0.172 ± 0.004	0.900 ± 0.011	15.772 ± 1.012	32.332 ± 1.132	0.192 ± 0.012	2.624
		p	0.188 ± 0.005	0.945 ± 0.011	24.132 ± 1.125	49.232 ± 1.321	0.075 ± 0.004	0.651
1(d)	80-92%	π^-	0.122 ± 0.004	0.900 ± 0.010	8.972 ± 0.559	28.132 ± 0.899	2.622 ± 0.165	2.234
		K^-	0.169 ± 0.004	0.900 ± 0.010	15.985 ± 1.009	32.032 ± 1.316	0.187 ± 0.011	1.305
		\bar{p}	0.188 ± 0.005	0.875 ± 0.011	21.032 ± 1.121	52.132 ± 1.325	0.057 ± 0.003	0.296
2(a)	0-5%	π^+	0.191 ± 0.004	0.880 ± 0.012	17.232 ± 1.121	34.832 ± 1.143	238.352 ± 16.151	13.195
		K^+	0.285 ± 0.005	0.945 ± 0.023	19.495 ± 1.122	29.232 ± 1.105	32.739 ± 3.015	0.345
		p	0.413 ± 0.005	0.995 ± 0.005	28.862 ± 1.515	29.258 ± 1.831	6.746 ± 0.312	2.387
2(b)	0-5%	π^-	0.191 ± 0.004	0.880 ± 0.012	17.232 ± 1.121	34.832 ± 1.143	245.352 ± 16.151	10.378
		K^-	0.280 ± 0.005	0.945 ± 0.023	19.495 ± 1.122	29.232 ± 1.105	33.139 ± 2.995	0.478
		\bar{p}	0.415 ± 0.005	0.997 ± 0.003	28.862 ± 1.515	29.258 ± 1.831	6.748 ± 0.311	1.799
2(c)	80-90%	π^+	0.139 ± 0.004	0.815 ± 0.025	16.232 ± 0.915	39.232 ± 1.115	3.125 ± 0.183	9.381
		K^+	0.197 ± 0.004	0.805 ± 0.029	18.072 ± 0.912	32.332 ± 1.545	0.331 ± 0.021	1.648
		p	0.266 ± 0.005	0.906 ± 0.021	26.132 ± 1.195	40.232 ± 1.625	0.100 ± 0.009	0.799
2(d)	80-90%	π^-	0.139 ± 0.004	0.815 ± 0.025	16.232 ± 0.915	39.232 ± 1.115	3.148 ± 0.185	8.652
		K^-	0.197 ± 0.004	0.815 ± 0.025	17.172 ± 0.903	30.332 ± 1.355	0.324 ± 0.019	2.211
		\bar{p}	0.261 ± 0.005	0.901 ± 0.021	28.132 ± 1.212	40.232 ± 1.715	0.099 ± 0.009	1.116

Table 5. Values of free parameters (T , q , k , p_0 , and n), normalization constant (N_0), and χ^2/dof corresponding to the fits of the Tsallis distribution and inverse power-law in Figures 1 and 2.

Fig.	Cent.	Part.	T (GeV)	q	k	p_0 (GeV/c)	n	N_0	χ^2/dof
1(a)	0-5%	π^+	0.128 ± 0.004	1.070 ± 0.003	0.996 ± 0.004	1.775 ± 0.065	7.975 ± 0.146	160.052 ± 9.121	0.942
		K^+	0.180 ± 0.005	1.049 ± 0.005	0.990 ± 0.005	1.175 ± 0.058	4.675 ± 0.135	18.602 ± 1.102	4.949
		p	0.273 ± 0.004	1.015 ± 0.003	0.997 ± 0.002	0.175 ± 0.005	0.275 ± 0.011	4.741 ± 0.101	5.613
1(b)	0-5%	π^-	0.127 ± 0.004	1.071 ± 0.003	0.997 ± 0.003	1.075 ± 0.075	8.975 ± 0.165	159.121 ± 10.232	0.522
		K^-	0.178 ± 0.005	1.052 ± 0.005	0.990 ± 0.005	1.075 ± 0.055	5.975 ± 0.178	17.642 ± 0.106	2.610
		\bar{p}	0.278 ± 0.005	1.013 ± 0.003	0.995 ± 0.004	0.306 ± 0.019	1.865 ± 0.096	3.501 ± 0.186	8.356
1(c)	80-92%	π^+	0.099 ± 0.004	1.085 ± 0.005	0.992 ± 0.005	2.485 ± 0.075	6.032 ± 0.146	2.412 ± 0.145	0.780
		K^+	0.124 ± 0.004	1.078 ± 0.004	0.993 ± 0.006	4.883 ± 0.099	5.153 ± 0.136	0.194 ± 0.012	2.200
		p	0.161 ± 0.005	1.024 ± 0.006	0.963 ± 0.008	1.906 ± 0.056	7.166 ± 0.155	0.078 ± 0.005	0.671
1(d)	80-92%	π^-	0.099 ± 0.004	1.086 ± 0.005	0.991 ± 0.004	2.435 ± 0.066	6.032 ± 0.146	2.402 ± 0.138	0.565
		K^-	0.121 ± 0.004	1.078 ± 0.004	0.991 ± 0.007	4.903 ± 0.103	5.353 ± 0.137	0.194 ± 0.012	0.903
		\bar{p}	0.164 ± 0.005	1.028 ± 0.006	0.963 ± 0.008	1.906 ± 0.056	7.176 ± 0.156	0.055 ± 0.004	0.214
2(a)	0-5%	π^+	0.164 ± 0.005	1.066 ± 0.005	0.989 ± 0.007	5.175 ± 0.162	7.975 ± 0.185	259.152 ± 20.052	6.821
		K^+	0.258 ± 0.006	1.030 ± 0.005	0.997 ± 0.002	3.475 ± 0.108	6.075 ± 0.226	34.202 ± 2.858	0.256
		p	0.409 ± 0.006	1.002 ± 0.001	0.998 ± 0.002	4.075 ± 0.102	6.875 ± 0.232	6.715 ± 0.292	2.676
2(b)	0-5%	π^-	0.164 ± 0.005	1.066 ± 0.005	0.989 ± 0.007	5.175 ± 0.162	7.975 ± 0.185	259.152 ± 20.052	6.788
		K^-	0.255 ± 0.006	1.029 ± 0.005	0.995 ± 0.004	3.475 ± 0.138	6.075 ± 0.232	34.202 ± 2.858	0.302
		\bar{p}	0.409 ± 0.006	1.002 ± 0.001	0.998 ± 0.002	4.075 ± 0.102	6.875 ± 0.232	6.715 ± 0.292	2.055
2(c)	80-90%	π^+	0.114 ± 0.004	1.099 ± 0.005	0.981 ± 0.007	5.575 ± 0.172	8.175 ± 0.196	3.151 ± 0.165	7.954
		K^+	0.170 ± 0.005	1.066 ± 0.005	0.948 ± 0.014	4.075 ± 0.134	6.875 ± 0.201	0.314 ± 0.018	1.303
		p	0.245 ± 0.005	1.024 ± 0.004	0.985 ± 0.005	6.875 ± 0.178	5.465 ± 0.135	0.099 ± 0.005	1.088
2(d)	80-90%	π^-	0.114 ± 0.004	1.099 ± 0.005	0.981 ± 0.007	5.575 ± 0.172	8.175 ± 0.196	3.159 ± 0.167	7.494
		K^-	0.167 ± 0.005	1.064 ± 0.005	0.952 ± 0.011	4.085 ± 0.130	6.815 ± 0.185	0.317 ± 0.021	1.897
		\bar{p}	0.235 ± 0.005	1.024 ± 0.005	0.981 ± 0.007	5.975 ± 0.154	5.365 ± 0.165	0.108 ± 0.008	1.393

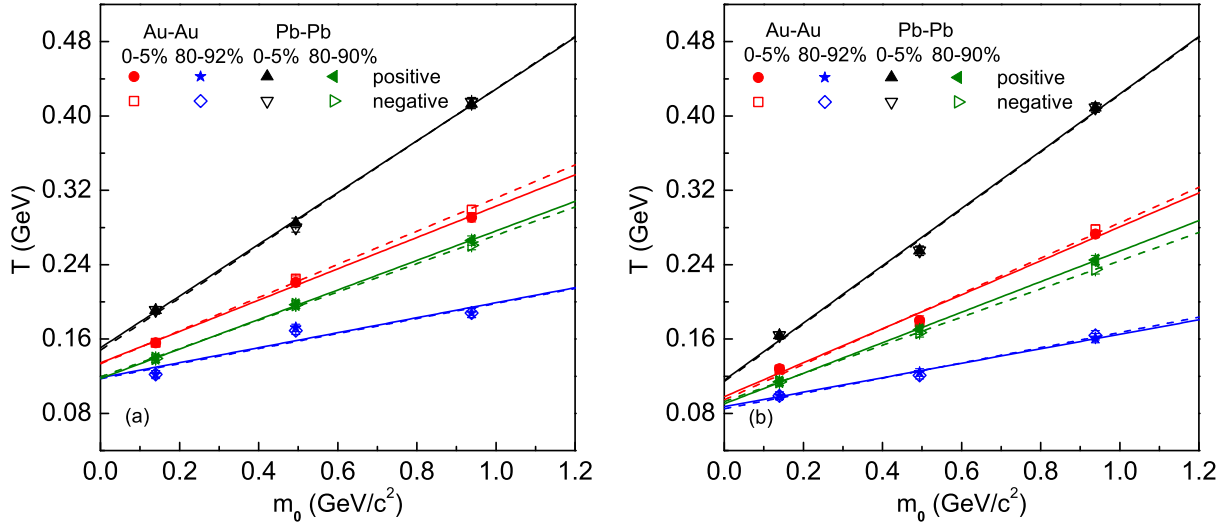


Fig. 3. Relations between T and m_0 . The symbols presented in panels (a) and (b) represent the results listed in Tables 4 and 5 and corresponded to the fits of Boltzmann and Tsallis distributions respectively, where the closed and open symbols show the results of positively and negatively charged particles respectively. The solid and dashed lines are the results fitted by the method of least squares for the positively and negatively charged particles respectively.

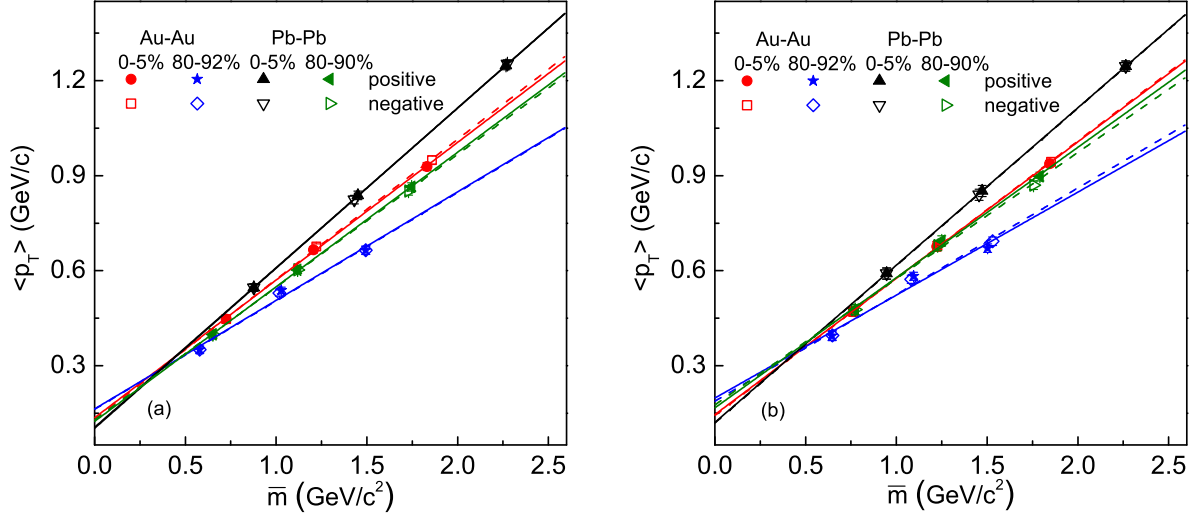


Fig. 4. Same as Figure 3, but showing the relations between $\langle p_T \rangle$ and \overline{m} . The symbols presented in panels (a) and (b) represent the results obtained according to the fits of Boltzmann and Tsallis distributions respectively, where the values of parameters are listed in Tables 4 and 5 respectively.

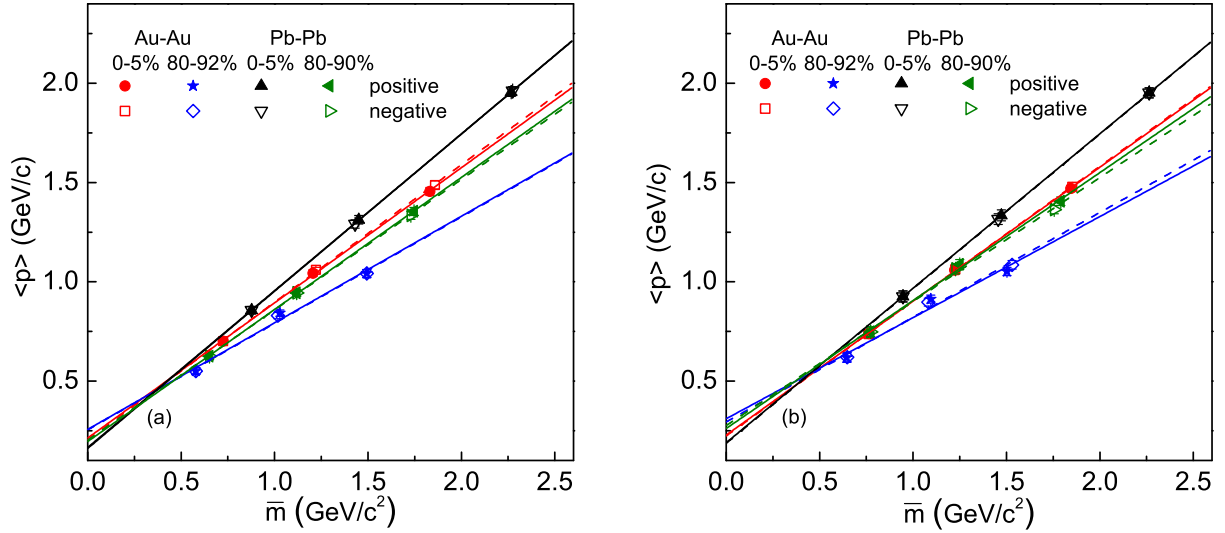


Fig. 5. Same as Figure 3, but showing the relations between $\langle p \rangle$ and \overline{m} . The symbols presented in panels (a) and (b) represent the results obtained according to the fits of Boltzmann and Tsallis distributions respectively, where the values of parameters are listed in Tables 4 and 5 respectively.

Table 6. Values of free parameters (intercept and slope) and χ^2/dof corresponding to the relations obtained from the fits of the Boltzmann distribution in Figures 3(a), 4(a), and 5(a).

Figure	Relation	Type	Centrality	Intercept	Slope	χ^2/dof		
3(a)	$T - m_0$	Au-Au	positive	0-5%	0.134 ± 0.003	0.169 ± 0.005	1.048	
			negative	0-5%	0.133 ± 0.004	0.179 ± 0.006	1.912	
			positive	80-92%	0.118 ± 0.013	0.081 ± 0.021	17.006	
		Pb-Pb	negative	80-92%	0.117 ± 0.011	0.081 ± 0.018	12.442	
			positive	0-5%	0.151 ± 0.003	0.278 ± 0.005	0.580	
			negative	0-5%	0.148 ± 0.006	0.281 ± 0.010	3.150	
				positive	80-90%	0.117 ± 0.001	0.159 ± 0.002	0.113
				negative	80-90%	0.119 ± 0.002	0.152 ± 0.004	0.605
4(a)	$\langle p_T \rangle - \bar{m}$	Au-Au	positive	0-5%	0.136 ± 0.009	0.435 ± 0.007	0.482	
			negative	0-5%	0.130 ± 0.009	0.442 ± 0.007	0.806	
			positive	80-92%	0.164 ± 0.032	0.343 ± 0.029	5.939	
		Pb-Pb	negative	80-92%	0.163 ± 0.028	0.342 ± 0.025	4.505	
			positive	0-5%	0.106 ± 0.001	0.504 ± 0.001	0.008	
			negative	0-5%	0.103 ± 0.003	0.505 ± 0.002	0.033	
				positive	80-90%	0.125 ± 0.005	0.425 ± 0.004	0.174
				negative	80-90%	0.129 ± 0.008	0.419 ± 0.006	0.363
5(a)	$\langle p \rangle - \bar{m}$	Au-Au	positive	0-5%	0.213 ± 0.014	0.681 ± 0.011	0.483	
			negative	0-5%	0.204 ± 0.015	0.693 ± 0.011	0.801	
			positive	80-92%	0.256 ± 0.050	0.537 ± 0.045	5.916	
		Pb-Pb	negative	80-92%	0.255 ± 0.043	0.536 ± 0.039	4.519	
			positive	0-5%	0.165 ± 0.002	0.790 ± 0.001	0.008	
			negative	0-5%	0.161 ± 0.004	0.792 ± 0.003	0.032	
				positive	80-90%	0.195 ± 0.008	0.665 ± 0.006	0.173
				negative	80-90%	0.202 ± 0.012	0.657 ± 0.009	0.361

Table 7. Values of free parameters (intercept and slope) and χ^2/dof corresponding to the relations obtained from the fits of the Tsallis distribution in Figures 3(b), 4(b), and 5(b).

Figure	Relation	Type	Centrality	Intercept	Slope	χ^2/dof		
3(b)	$T - m_0$	Au-Au	positive	0-5%	0.098 ± 0.008	0.183 ± 0.013	4.766	
			negative	0-5%	0.095 ± 0.010	0.191 ± 0.016	7.533	
			positive	80-92%	0.087 ± 0.002	0.078 ± 0.003	0.245	
		Pb-Pb	negative	80-92%	0.085 ± 0.004	0.082 ± 0.007	1.838	
			positive	0-5%	0.116 ± 0.009	0.308 ± 0.015	4.299	
			negative	0-5%	0.114 ± 0.011	0.308 ± 0.018	6.244	
				positive	80-90%	0.090 ± 0.001	0.164 ± 0.002	0.128
				negative	80-90%	0.093 ± 0.001	0.152 ± 0.001	0.012
4(b)	$\langle p_T \rangle - \bar{m}$	Au-Au	positive	0-5%	0.146 ± 0.006	0.431 ± 0.005	0.129	
			negative	0-5%	0.143 ± 0.006	0.433 ± 0.005	0.121	
			positive	80-92%	0.198 ± 0.047	0.325 ± 0.041	7.275	
		Pb-Pb	negative	80-92%	0.188 ± 0.033	0.337 ± 0.029	3.795	
			positive	0-5%	0.121 ± 0.001	0.497 ± 0.001	0.003	
			negative	0-5%	0.119 ± 0.005	0.497 ± 0.003	0.044	
				positive	80-90%	0.167 ± 0.022	0.411 ± 0.016	1.146
				negative	80-90%	0.177 ± 0.021	0.399 ± 0.016	1.092
5(b)	$\langle p \rangle - \bar{m}$	Au-Au	positive	0-5%	0.228 ± 0.010	0.675 ± 0.007	0.130	
			negative	0-5%	0.224 ± 0.010	0.679 ± 0.007	0.122	
			positive	80-92%	0.310 ± 0.073	0.509 ± 0.065	7.274	
		Pb-Pb	negative	80-92%	0.295 ± 0.052	0.528 ± 0.045	3.812	
			positive	0-5%	0.189 ± 0.002	0.778 ± 0.001	0.003	
			negative	0-5%	0.187 ± 0.007	0.779 ± 0.004	0.043	
				positive	80-90%	0.261 ± 0.034	0.644 ± 0.025	1.145
				negative	80-90%	0.276 ± 0.034	0.625 ± 0.026	1.101

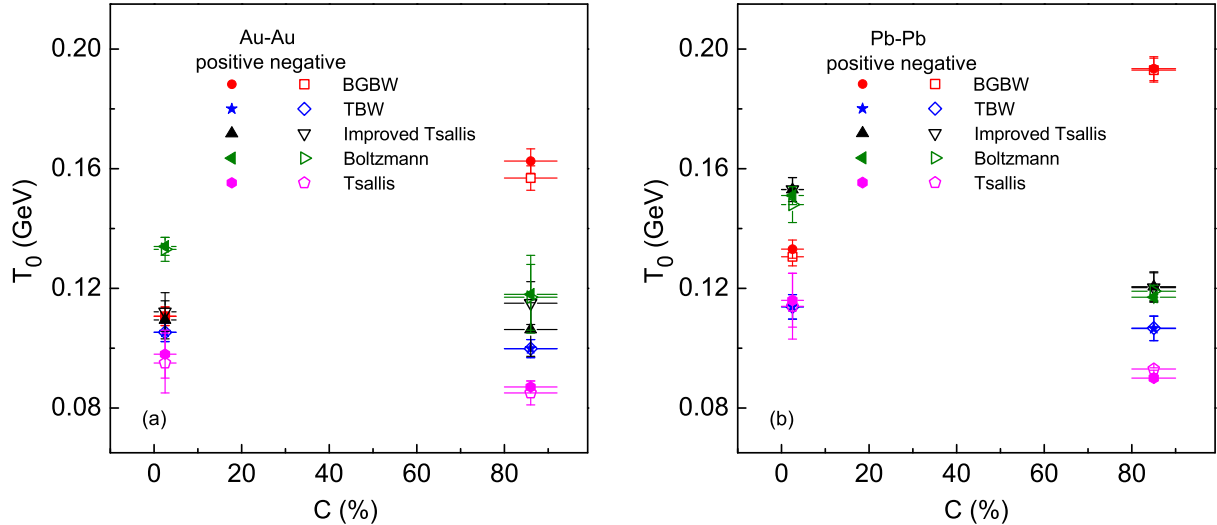


Fig. 6. Comparisons of T_0 obtained by different methods for different centralities (C). Panels (a) and (b) correspond to the results for 0–5% and 80–92% Au-Au collisions at $\sqrt{s_{NN}} = 200$ GeV and 0–5% and 80–90% Pb-Pb collisions at $\sqrt{s_{NN}} = 2.76$ TeV respectively, where the values of T_0 in the first three methods are obtained by weighting different particles.

and χ^2/dof are listed in Tables 6 and 7 which correspond to the methods iv)_a and iv)_b respectively. One can see that, in most cases, the mentioned relations are described by a linear function. In particular, the intercept in Figure 3 is regarded as T_0 , and the slopes in Figures 4 and 5 are regarded as β_T and β respectively. The values of T , T_0 , β_T , β , and \bar{m} are approximately independent of isospin.

To compare values of key parameters obtained by different methods for different centralities (both central and peripheral collisions), Figures 6 and 7 show T_0 and β_T respectively, where panels (a) and (b) correspond to the results for 0–5% and 80–92% Au-Au collisions at $\sqrt{s_{NN}} = 200$ GeV and 0–5% and 80–90% Pb-Pb collisions at $\sqrt{s_{NN}} = 2.76$ TeV respectively. The closed and open symbols represent positive and negative charged particles respectively, which are quoted from Tables 1, 2, 3, 6, and 7 which correspond to the methods i), ii), iii), iv)_a, and iv)_b, respectively. In particular, the values of T_0 and β_T in the first three methods are obtained by weighting different particles. One can see that, by using the method i), the value of T_0 in central collisions is less than that in peripheral collisions, and other methods present a larger T_0 in central collisions. The methods i) and ii) show a nearly zero β_T in peripheral collisions according to refs. [11, 14], while other methods show

a considerable β_T in both central and peripheral collisions.

To explain the inconsistent results in T_0 and β_T for different methods, we re-examine the first two methods. It should be noticed that the same flow profile function $\beta(r) = \beta_S(r/R)^{n_0}$ is used in the first two methods, though $n_0 = 2$ is used in the method i) [11] and $n_0 = 1$ is used in the method ii) [14] with the traditional treatment. The radial size R of the thermal source in central collisions can be approximately regarded as the radius of a collision nucleus. However, in peripheral collisions, the radial size R of the thermal source should not be zero due to a few participant nucleons taking part in the interactions. Even in ultra-peripheral collisions, the radial size R of the thermal source should not be less than the radius of a nucleus. In the considered peripheral (80–90% or 80–92%) collisions, we can take approximately R to be 2.5 fm due to the thermal source containing a few nucleons. The consideration of non-zero R , thus the non-zero β_T , in peripheral collisions is a new treatment by us for the methods i) and ii). In the concrete calculation, R is not a sensitive quantity.

After the new treatment for the peripheral collisions in the first two methods, we re-analyze the data presented in Figures 1 and 2. At the same time, to see the influences of different n_0 in the self-similar flow pro-

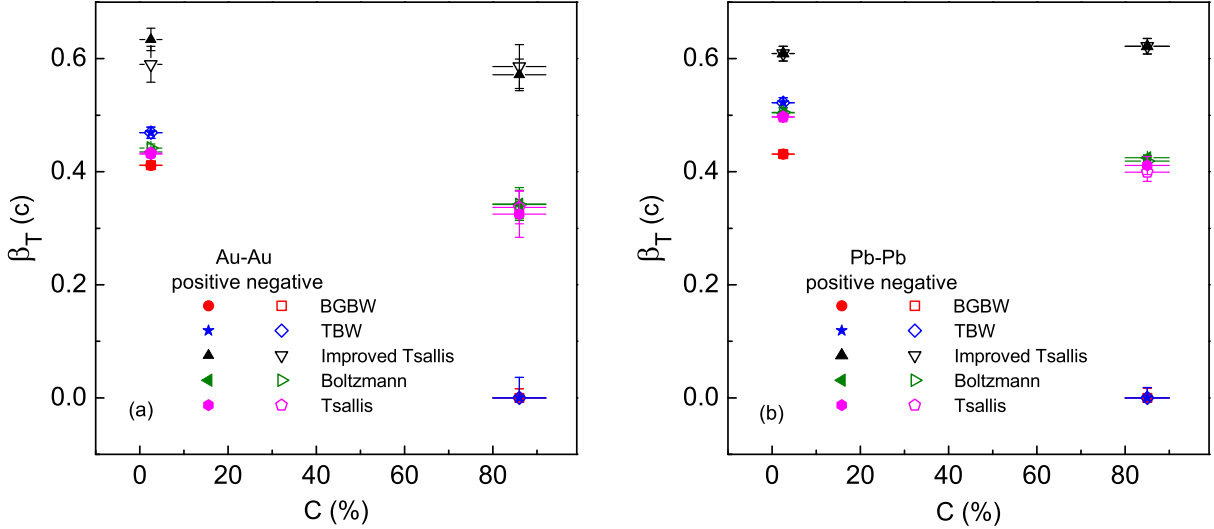


Fig. 7. Same as Figure 6, but showing the comparisons of β_T obtained by different methods for different centralities.

file, we refit the mentioned p_T spectra by the first two methods with $n_0 = 1$ and 2 synchronously. The results re-analyzed by us are shown in Figures 8 and 9 which correspond to 200 GeV Au-Au and 2.76 TeV Pb-Pb collisions respectively. The data points are the same as Figures 1 and 2 [26, 28]. The dotted, solid, dashed, and dotted-dashed curves correspond to the results of the method i) with $n_0 = 1$ and 2, and of the method ii) with $n_0 = 1$ and 2, respectively, where the results of the method i) with $n_0 = 2$ and of the method ii) with $n_0 = 1$ in central collisions are the same as Figures 1 and 2. The values of related parameters and χ^2/dof are listed in Tables 8 and 9, where the parameters for the method i) with $n_0 = 2$ and for the method ii) with $n_0 = 1$ in central collisions repeat those in Tables 1 and 2, which are not listed again. One can see that, after the re-examination, the values of T_0 in central collisions are greater than those in peripheral collisions. The values of β_T in peripheral collisions are no longer zero. These new results are consistent with other methods.

To give new comparisons for T_0 and β_T , the new results obtained by the first two methods are shown in Figures 10 and 11 respectively, where the results corresponding to the method i) for central collisions with $n_0 = 2$ and to the method ii) for central collisions with $n_0 = 1$ are the same as those in Figures 6 and 7. Combining Figures 6, 7, 10, and 11, One can see that the four methods show approximately the consistent re-

sults. These comparisons enlighten us to use the first two methods in peripheral collisions by a non-zero R which performs a non-zero β_T . After the re-examination for R in peripheral collisions, we obtain a slightly larger T_0 in central collisions for the four methods. In particular, the parameter T_0 at the LHC is slightly larger than that at the RHIC, not only for central collisions but also for peripheral collisions. Except the method iii), other methods show a slightly larger β_T in central collisions and at the LHC, while the method iii) shows a nearly the same β_T in different centralities and at different energies.

Comparing with peripheral collisions, the larger T_0 in central collisions renders more deposition of collision energy and higher excitation of interacting system due to more participant nucleons taking part in the violent collisions. Comparing with the top RHIC energy, the larger T_0 at the LHC energy also renders more deposition of collision energy and higher excitation of interacting system due to higher $\sqrt{s_{NN}}$ at the LHC. At the same time, from the top RHIC to the LHC energies, a slight increase in T_0 reflects the limiting deposition of collision energy. Comparing with peripheral collisions, the slight larger or nearly the same β_T in central collisions renders similar expansion in both the centralities. At the same time, at the top RHIC and the LHC energies, the two systems also show similar expansion due to similar β_T .

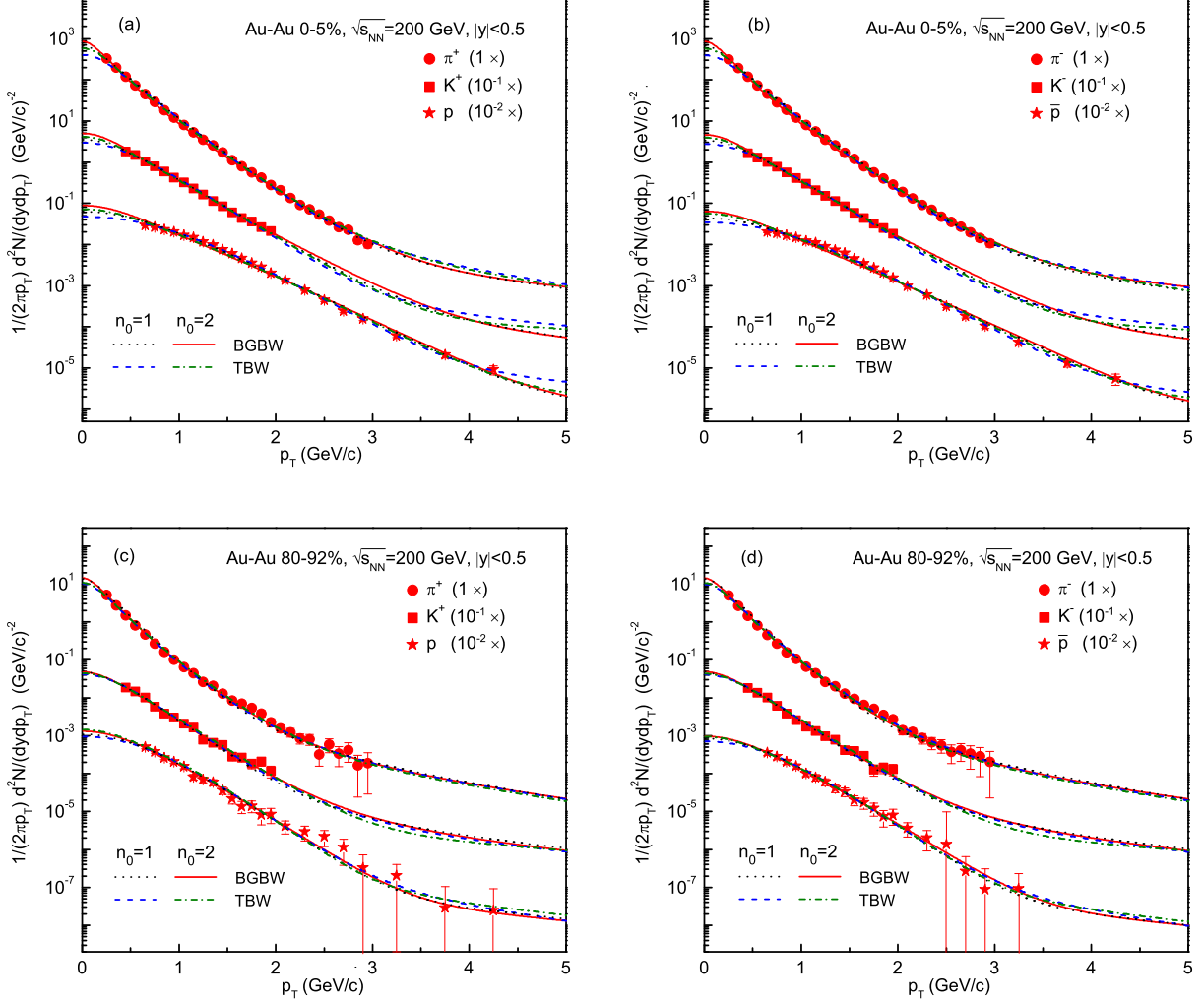


Fig. 8. Reanalyzing the transverse momentum spectra of (a)-(c) π^+ , K^+ , and p , as well as (b)-(d) π^- , K^- , and \bar{p} produced in (a)-(b) 0-5% and (c)-(d) 80-92% Au-Au collisions at $\sqrt{s_{NN}} = 200$ GeV by the first two methods. The symbols represent the same experimental data as Figure 1 [26]. The dotted, solid, dashed, and dotted-dashed curves are our results calculated by using the method i) with $n_0 = 1$ and 2, as well as the method ii) with $n_0 = 1$ and 2, respectively. The results for central collisions obtained by the method i) with $n_0 = 2$ and by the method ii) with $n_0 = 1$ are the same as Figure 1.

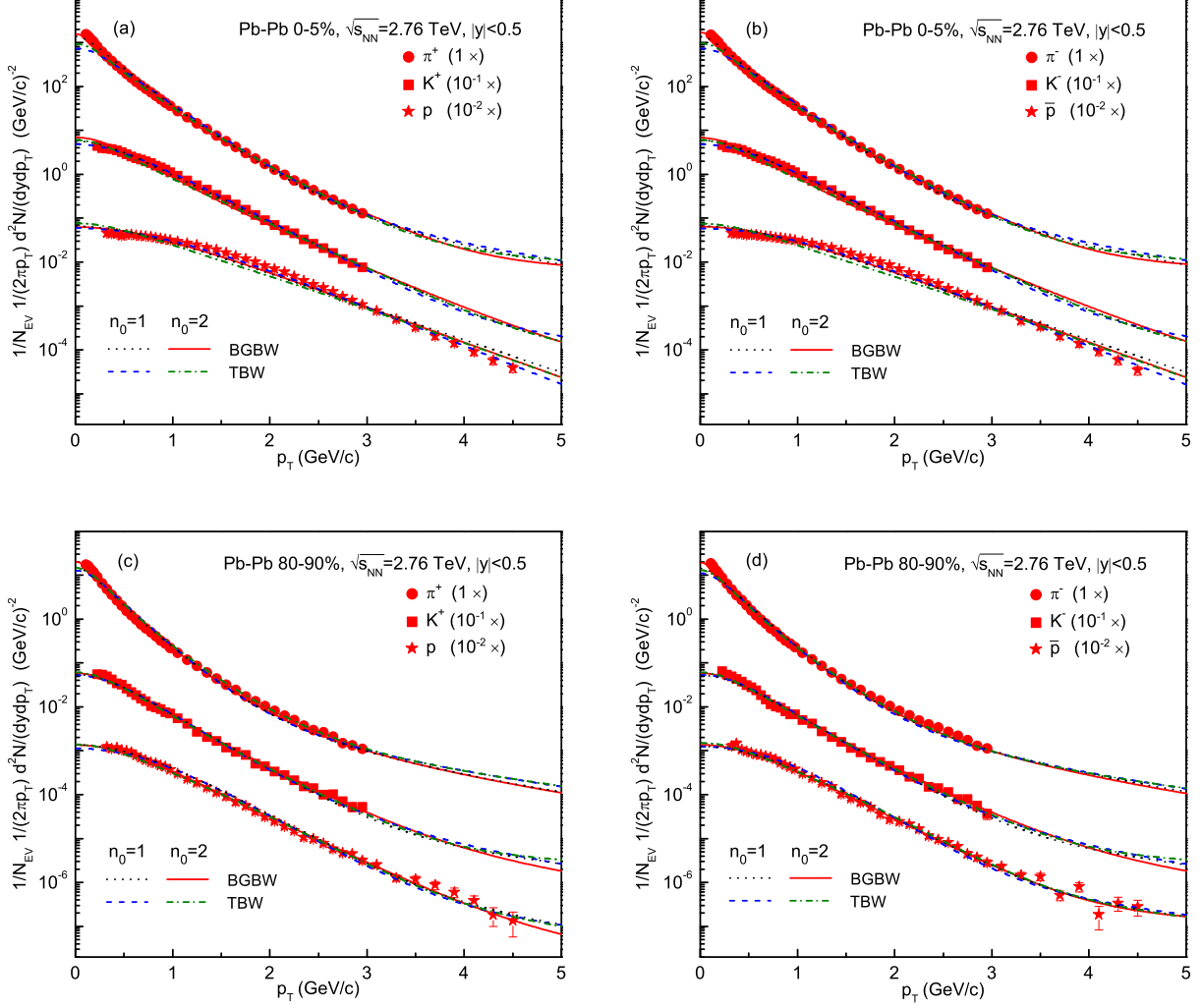


Fig. 9. Same as Figure 8, but showing the spectra in (a)-(b) 0–5% and (c)-(d) 80–90% Pb-Pb collisions at $\sqrt{s_{NN}} = 2.76$ TeV. The symbols represent the same experimental data as Figure 2 [28]. The results for central collisions obtained by the method i) with $n_0 = 2$ and by the method ii) with $n_0 = 1$ are the same as Figure 2.

Table 8. Values of free parameters (T_0 , β_T , k , p_0 , and n), normalization constant (N_0), and χ^2/dof corresponding to the fits of the BGBW model and inverse power-law in Figures 8 and 9, where the values for 0–5% collisions with $n_0 = 2$ in the self-similar flow profile repeat those in Table 1, which are not listed again.

Fig.	Cent.	Part.	T_0 (GeV)	β_T (c)	k	p_0 (GeV/c)	n	N_0	χ^2/dof
8(a)	0–5%	π^+	0.138 ± 0.005	0.429 ± 0.008	0.990 ± 0.004	0.559 ± 0.024	4.097 ± 0.185	198.885 ± 15.883	1.281
Au-Au		K^+	0.169 ± 0.005	0.412 ± 0.008	0.992 ± 0.004	4.909 ± 0.116	7.097 ± 0.205	19.075 ± 1.445	4.307
$n_0 = 1$		p	0.198 ± 0.006	0.398 ± 0.008	0.998 ± 0.002	6.175 ± 0.265	3.865 ± 0.119	5.985 ± 0.365	8.455
8(b)	0–5%	π^-	0.138 ± 0.005	0.428 ± 0.008	0.990 ± 0.004	0.519 ± 0.023	4.097 ± 0.187	199.465 ± 15.965	0.976
		K^-	0.169 ± 0.005	0.412 ± 0.008	0.992 ± 0.004	4.909 ± 0.116	7.097 ± 0.205	18.015 ± 1.365	2.167
		\bar{p}	0.198 ± 0.006	0.404 ± 0.008	0.998 ± 0.002	6.175 ± 0.265	3.865 ± 0.119	3.575 ± 0.285	11.650
8(c)	80–92%	π^+	0.115 ± 0.005	0.385 ± 0.010	0.980 ± 0.005	1.889 ± 0.209	6.547 ± 0.393	3.475 ± 0.126	2.695
		K^+	0.137 ± 0.005	0.375 ± 0.010	0.925 ± 0.012	0.429 ± 0.055	3.697 ± 0.161	0.209 ± 0.028	2.483
		p	0.143 ± 0.006	0.335 ± 0.010	0.994 ± 0.002	0.799 ± 0.066	3.197 ± 0.198	0.070 ± 0.007	0.947
8(d)	80–92%	π^-	0.115 ± 0.005	0.385 ± 0.010	0.980 ± 0.005	1.889 ± 0.209	6.547 ± 0.393	3.475 ± 0.126	2.818
		K^-	0.139 ± 0.005	0.378 ± 0.010	0.925 ± 0.012	0.429 ± 0.055	3.697 ± 0.161	0.198 ± 0.026	1.192
		\bar{p}	0.143 ± 0.006	0.335 ± 0.010	0.994 ± 0.002	0.699 ± 0.063	3.197 ± 0.198	0.054 ± 0.005	0.234
8(c)	80–92%	π^+	0.103 ± 0.005	0.375 ± 0.010	0.955 ± 0.009	0.569 ± 0.026	4.647 ± 0.215	3.375 ± 0.265	0.685
Au-Au		K^+	0.117 ± 0.006	0.375 ± 0.010	0.955 ± 0.010	0.739 ± 0.031	3.997 ± 0.195	0.207 ± 0.010	2.140
$n_0 = 2$		p	0.118 ± 0.006	0.325 ± 0.010	0.995 ± 0.004	0.799 ± 0.037	3.197 ± 0.155	0.078 ± 0.005	0.743
8(d)	80–92%	π^-	0.103 ± 0.005	0.375 ± 0.010	0.955 ± 0.009	0.569 ± 0.026	4.647 ± 0.215	3.315 ± 0.261	0.591
		K^-	0.115 ± 0.006	0.375 ± 0.010	0.955 ± 0.010	0.739 ± 0.031	3.997 ± 0.195	0.207 ± 0.010	0.801
		\bar{p}	0.122 ± 0.006	0.325 ± 0.010	0.995 ± 0.004	0.799 ± 0.037	3.197 ± 0.155	0.058 ± 0.005	0.140
9(a)	0–5%	π^+	0.149 ± 0.005	0.458 ± 0.009	0.970 ± 0.006	2.109 ± 0.095	6.297 ± 0.118	441.385 ± 36.396	5.600
Pb-Pb		K^+	0.235 ± 0.005	0.399 ± 0.009	0.997 ± 0.003	4.509 ± 0.105	4.597 ± 0.113	35.875 ± 3.559	0.835
$n_0 = 1$		p	0.355 ± 0.005	0.347 ± 0.009	0.999 ± 0.001	4.309 ± 0.126	3.297 ± 0.102	6.585 ± 0.229	9.730
9(b)	0–5%	π^-	0.149 ± 0.005	0.458 ± 0.009	0.970 ± 0.006	2.109 ± 0.095	6.297 ± 0.118	411.565 ± 35.456	4.852
		K^-	0.235 ± 0.005	0.397 ± 0.009	0.997 ± 0.003	4.509 ± 0.105	4.597 ± 0.113	37.455 ± 3.615	0.613
		\bar{p}	0.355 ± 0.005	0.347 ± 0.009	0.999 ± 0.001	4.309 ± 0.126	3.297 ± 0.102	6.724 ± 0.236	7.329
9(c)	80–90%	π^+	0.127 ± 0.005	0.448 ± 0.010	0.942 ± 0.008	1.509 ± 0.089	5.647 ± 0.183	4.185 ± 0.188	9.316
		K^+	0.169 ± 0.004	0.448 ± 0.008	0.980 ± 0.010	2.909 ± 0.102	4.997 ± 0.148	0.310 ± 0.018	2.159
		p	0.180 ± 0.005	0.408 ± 0.010	0.981 ± 0.007	6.909 ± 0.185	8.997 ± 0.196	0.102 ± 0.008	1.403
9(d)	80–90%	π^-	0.129 ± 0.005	0.448 ± 0.010	0.940 ± 0.008	1.509 ± 0.089	5.647 ± 0.183	4.085 ± 0.186	8.730
		K^-	0.169 ± 0.004	0.448 ± 0.008	0.980 ± 0.010	2.909 ± 0.102	4.997 ± 0.148	0.296 ± 0.016	2.628
		\bar{p}	0.178 ± 0.005	0.408 ± 0.010	0.981 ± 0.007	6.909 ± 0.185	6.697 ± 0.176	0.099 ± 0.008	1.488
9(c)	80–90%	π^+	0.113 ± 0.004	0.395 ± 0.008	0.950 ± 0.006	1.509 ± 0.088	5.647 ± 0.132	5.185 ± 0.181	6.788
Pb-Pb		K^+	0.184 ± 0.005	0.365 ± 0.008	0.978 ± 0.006	1.909 ± 0.098	4.997 ± 0.155	0.320 ± 0.018	1.457
$n_0 = 2$		p	0.204 ± 0.005	0.325 ± 0.008	0.991 ± 0.005	6.909 ± 0.198	8.997 ± 0.126	0.102 ± 0.009	0.893
9(d)	80–90%	π^-	0.113 ± 0.004	0.398 ± 0.008	0.950 ± 0.006	1.509 ± 0.088	5.647 ± 0.132	4.985 ± 0.177	5.271
		K^-	0.184 ± 0.005	0.365 ± 0.008	0.978 ± 0.006	1.909 ± 0.098	4.997 ± 0.155	0.321 ± 0.018	2.122
		\bar{p}	0.204 ± 0.005	0.314 ± 0.008	0.988 ± 0.005	6.909 ± 0.198	3.197 ± 0.126	0.102 ± 0.009	0.888

Table 9. Values of free parameters (T_0 , q , β_T , k , p_0 , and n), normalization constant (N_0), and χ^2/dof corresponding to the fits of the TBW model and inverse power-law in Figures 8 and 9, where the values for 0–5% collisions with $n_0 = 1$ in the self-similar flow profile repeat those in Table 2, which are not listed again.

Fig.	Cent.	Part.	T_0 (GeV)	q	β_T (c)	k	p_0 (GeV/c)	n	N_0	χ^2/dof
8(c)	80–92%	π^+	0.079 ± 0.004	1.065 ± 0.006	0.375 ± 0.016	0.991 ± 0.004	3.097 ± 0.109	6.909 ± 0.236	2.752 ± 0.211	0.926
Au-Au		K^+	0.084 ± 0.005	1.056 ± 0.005	0.375 ± 0.016	0.985 ± 0.006	2.431 ± 0.096	4.858 ± 0.165	0.197 ± 0.019	2.789
$n_0 = 1$		p	0.085 ± 0.005	1.026 ± 0.005	0.375 ± 0.016	0.991 ± 0.003	4.251 ± 0.102	7.958 ± 0.235	0.066 ± 0.005	1.316
8(d)	80–92%	π^-	0.079 ± 0.004	1.065 ± 0.006	0.375 ± 0.016	0.992 ± 0.004	3.097 ± 0.109	6.909 ± 0.236	2.752 ± 0.211	0.966
		K^-	0.084 ± 0.005	1.056 ± 0.005	0.375 ± 0.016	0.985 ± 0.006	2.431 ± 0.096	4.858 ± 0.165	0.195 ± 0.018	1.481
		\bar{p}	0.085 ± 0.005	1.026 ± 0.005	0.375 ± 0.016	0.991 ± 0.003	4.251 ± 0.102	7.958 ± 0.235	0.049 ± 0.005	0.277
8(a)	0–5%	π^+	0.091 ± 0.003	1.010 ± 0.005	0.401 ± 0.008	0.995 ± 0.003	2.597 ± 0.087	6.209 ± 0.183	182.852 ± 12.652	0.513
Au-Au		K^+	0.103 ± 0.005	1.008 ± 0.004	0.395 ± 0.007	0.995 ± 0.004	3.097 ± 0.103	2.109 ± 0.089	20.652 ± 1.955	4.489
$n_0 = 2$		p	0.118 ± 0.005	1.009 ± 0.004	0.378 ± 0.005	0.997 ± 0.002	5.437 ± 0.168	2.809 ± 0.108	5.252 ± 0.228	13.177
8(b)	0–5%	π^-	0.091 ± 0.003	1.010 ± 0.005	0.401 ± 0.008	0.996 ± 0.003	2.597 ± 0.087	6.209 ± 0.183	182.352 ± 12.652	0.148
		K^-	0.103 ± 0.005	1.008 ± 0.004	0.395 ± 0.007	0.995 ± 0.004	3.097 ± 0.103	2.109 ± 0.089	19.752 ± 1.903	5.483
		\bar{p}	0.117 ± 0.005	1.009 ± 0.004	0.377 ± 0.005	0.997 ± 0.002	5.437 ± 0.168	2.809 ± 0.108	4.092 ± 0.203	17.397
8(c)	80–92%	π^+	0.073 ± 0.004	1.025 ± 0.004	0.395 ± 0.008	0.990 ± 0.004	2.797 ± 0.091	6.909 ± 0.185	2.852 ± 0.205	0.898
		K^+	0.082 ± 0.005	1.028 ± 0.005	0.375 ± 0.008	0.992 ± 0.005	2.031 ± 0.083	2.958 ± 0.114	0.202 ± 0.019	3.321
		p	0.085 ± 0.005	1.003 ± 0.002	0.342 ± 0.008	0.990 ± 0.004	1.051 ± 0.068	3.958 ± 0.139	0.078 ± 0.006	1.045
8(d)	80–92%	π^-	0.073 ± 0.004	1.025 ± 0.004	0.395 ± 0.008	0.990 ± 0.004	2.797 ± 0.091	6.909 ± 0.185	2.792 ± 0.201	0.680
		K^-	0.082 ± 0.005	1.028 ± 0.005	0.375 ± 0.008	0.992 ± 0.005	2.031 ± 0.083	2.958 ± 0.114	0.197 ± 0.017	1.600
		\bar{p}	0.088 ± 0.005	1.003 ± 0.002	0.344 ± 0.008	0.990 ± 0.004	1.051 ± 0.068	3.958 ± 0.139	0.056 ± 0.005	0.188
9(c)	80–90%	π^+	0.089 ± 0.004	1.041 ± 0.005	0.441 ± 0.010	0.965 ± 0.006	1.685 ± 0.065	5.059 ± 0.122	4.112 ± 0.165	15.362
Pb-Pb		K^+	0.099 ± 0.005	1.057 ± 0.005	0.441 ± 0.010	0.978 ± 0.006	5.931 ± 0.115	8.258 ± 0.185	0.308 ± 0.028	2.069
$n_0 = 1$		p	0.106 ± 0.005	1.028 ± 0.005	0.441 ± 0.010	0.980 ± 0.007	2.551 ± 0.102	4.958 ± 0.105	0.098 ± 0.008	2.547
9(d)	80–90%	π^-	0.089 ± 0.004	1.041 ± 0.005	0.452 ± 0.010	0.965 ± 0.006	1.685 ± 0.065	5.059 ± 0.122	3.631 ± 0.146	11.316
		K^-	0.099 ± 0.005	1.055 ± 0.005	0.441 ± 0.010	0.978 ± 0.006	5.931 ± 0.115	8.258 ± 0.185	0.309 ± 0.030	2.781
		\bar{p}	0.103 ± 0.005	1.020 ± 0.005	0.441 ± 0.010	0.965 ± 0.006	2.551 ± 0.102	4.958 ± 0.105	0.106 ± 0.009	2.932
9(a)	0–5%	π^+	0.099 ± 0.005	1.006 ± 0.004	0.435 ± 0.006	0.995 ± 0.003	3.097 ± 0.106	2.409 ± 0.092	338.042	

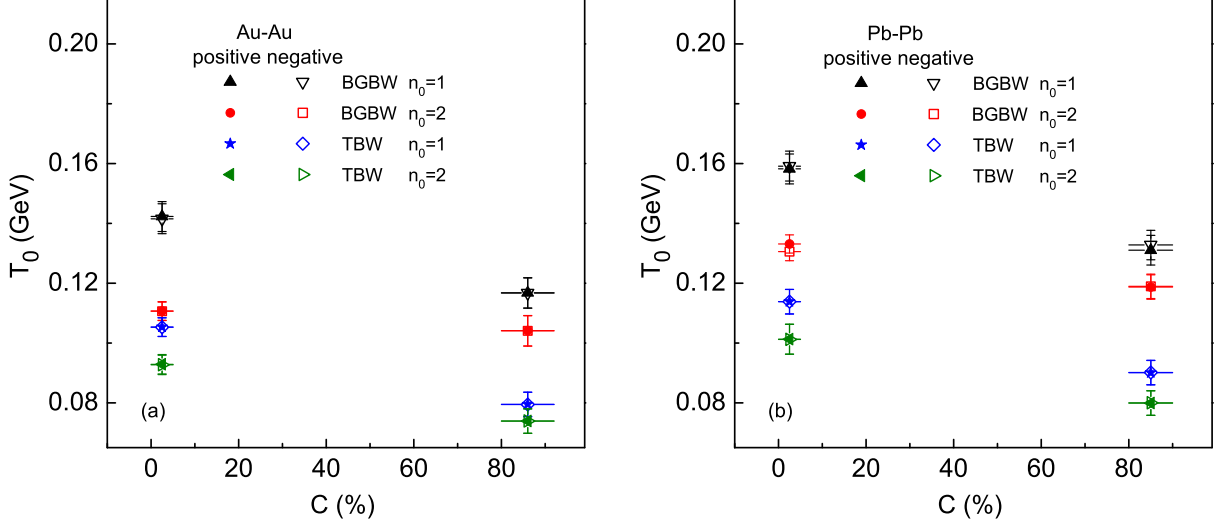


Fig. 10. Comparisons of T_0 obtained by the first two methods with $n_0 = 1$ and 2 for different centralities. Panels (a) and (b) correspond to the results for 0–5% and 80–92% Au-Au collisions at $\sqrt{s_{NN}} = 200$ GeV and 0–5% and 80–90% Pb-Pb collisions at $\sqrt{s_{NN}} = 2.76$ TeV respectively, where the values of T_0 are obtained by weighting different particles, and the results for central collisions obtained by the method i) with $n_0 = 2$ and by the method ii) with $n_0 = 1$ are the same as Figure 6.

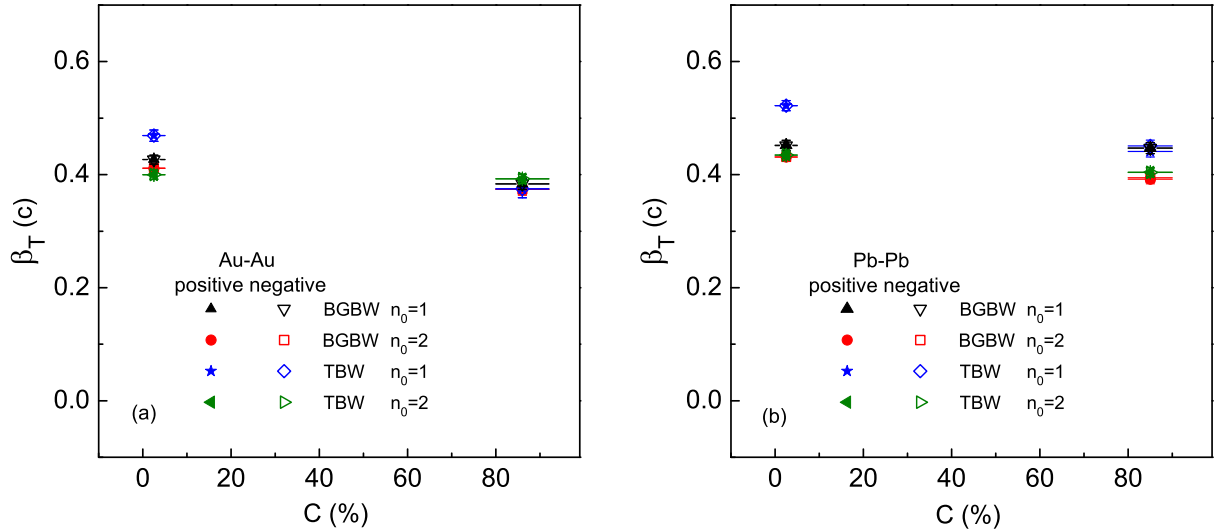


Fig. 11. Same as Figure 10, but showing the comparisons of β_T obtained by the first two methods for different centralities. The results for central collisions obtained by the method i) with $n_0 = 2$ and by the method ii) with $n_0 = 1$ are the same as Figure 7.

4 Conclusions

We summarize here our main observations and conclusions.

(a) The p_T spectra of π^\pm , K^\pm , p , and \bar{p} produced in 0–5% and 80–92% Au-Au collisions at $\sqrt{s_{NN}} = 200$ GeV and in 0–5% and 80–90% Pb-Pb collisions at $\sqrt{s_{NN}} = 2.76$ TeV have been analyzed by a few different superpositions in which the distributions related to the extractions of T_0 and β_T are used for the soft component and the inverse power law is used for the hard component. We have used five distributions, i) the Blast-Wave model with Boltzmann-Gibbs statistics, ii) the Blast-Wave model with Tsallis statistics, iii) the Tsallis distribution with flow effect, iv)_a the Boltzmann distribution, and iv)_b the Tsallis distribution, for the soft component. The first three distributions are in fact three methods for the extractions of T_0 and β_T . The last two distributions are used in the fourth method, i.e. the alternative method.

(b) The experimental data measured by the PHENIX and ALICE Collaborations are fitted by the modelling results. Our calculations show that the parameter T_0 obtained by the method i) with the traditional treatment for central collisions is less than that for peripheral collisions, which is inconsistent with the results obtained by other modelling methods. In the traditional treatment, the parameter β_T in peripheral collisions is taken to be nearly zero, which results from a zero radial size of the thermal source and results in a larger T_0 than normal case. By using the traditional treatment, both the methods i) and ii) show a nearly zero β_T in peripheral collisions according to refs. [11, 14], while other methods show a considerable β_T in both central and peripheral collisions.

(c) We have used a new treatment for peripheral collisions in the methods i) and ii). In the new treatment, a non-zero radial size of the thermal source, thus a non-zero β_T , for peripheral collisions is used. Even for ultra-peripheral collisions, the radial size is taken to be at least the radius of a nucleon. By using the new treatment, the first two methods show approximately consistent results with other methods, not only for T_0 but also for β_T , though the method iii) gives a larger β_T . We have uniformly obtained a slightly larger T_0 in

central collisions by the four methods. In particular, the parameter T_0 at the LHC is slightly larger than that at the RHIC. Except the method iii), other methods show a slightly larger β_T in central collisions and at the LHC.

Conflict of Interests

The authors declare that there is no conflict of interests regarding the publication of this paper.

Acknowledgments

This work was supported by the National Natural Science Foundation of China under Grant No. 11575103.

References

- [1] N. Xu (for the STAR Collaboration), Nucl. Phys. A **931**, 1 (2014).
- [2] S. Chatterjee, S. Das, L. Kumar, D. Mishra, B. Mohanty, R. Sahoo, and N. Sharma, Adv. High Energy Phys. **2015**, 349013 (2015).
- [3] S. Chatterjee, B. Mohanty, and R. Singh, Phys. Rev. C **92**, 024917 (2015).
- [4] S. Chatterjee and B. Mohanty, Phys. Rev. C **90**, 034908 (2014).
- [5] S. S. Räsänen (for the ALICE Collaboration), Proceedings of ICFNP 2015, arXiv:1603.03320v1 [nucl-ex] (2016).
- [6] M. Floris, Nucl. Phys. A **931**, 103 (2014).
- [7] S. Das, D. Mishra, S. Chatterjee, and B. Mohanty, Phys. Rev. C **95**, 014912 (2017).
- [8] P. Huovinen, Eur. Phys. J. A **37**, 121 (2008).
- [9] B. De, Eur. Phys. J. A **50**, 138 (2014).
- [10] A. Andronic, Int. J. Mod. Phys. A **29**, 1430047 (2014).
- [11] E. Schnedermann, J. Sollfrank, and U. Heinz, Phys. Rev. C **48**, 2462 (1993)
- [12] B. I. Abelev *et al.* (STAR Collaboration), Phys. Rev. C **79**, 034909 (2009)
- [13] B. I. Abelev *et al.* (STAR Collaboration), Phys. Rev. C **81**, 024911 (2010).
- [14] Z. B. Tang, Y. C. Xu, L. J. Ruan, G. van Buren, F. Q. Wang, and Z. B. Xu, Phys. Rev. C **79**, 051901(R) (2009).
- [15] T. Bhattacharyya, J. Cleymans, A. Khuntia, P. Pareek, and R. Sahoo, Eur. Phys. J. A **52**, 30 (2016).
- [16] D. Thakur, S. Tripathy, P. Garg, R. Sahoo, and J. Cleymans, Adv. High Energy Phys. **2016**, 4149352 (2016).
- [17] S. Takeuchi, K. Murase, T. Hirano, P. Huovinen, and Y. Nara, Phys. Rev. C **92**, 044907 (2015).

- [18] H. Heiselberg and A. M. Levy, Phys. Rev. C **59**, 2716 (1999).
- [19] U. W. Heinz, Lecture Notes for lectures presented at the 2nd CERN–Latin-American School of High-Energy Physics, June 1-14, 2003, San Miguel Regla, Mexico, arXiv:hep-ph/0407360v1 (2004).
- [20] R. Russo, Measurement of D^+ meson production in p-Pb collisions with the ALICE detector, PhD Thesis, Universita degli Studi di Torino, Italy, arXiv:1511.04380v1 [nucl-ex] (2015).
- [21] F.-H. Liu, Y.-Q. Gao, and H.-R. Wei, Adv. High Energy Phys. **2014**, 293873 (2014).
- [22] H.-R. Wei, F.-H. Liu, and R. A. Lacey, Eur. Phys. J. A **52**, 102 (2016).
- [23] H.-L. Lao, H.-R. Wei, F.-H. Liu, and R. A. Lacey, Eur. Phys. J. A **52**, 203 (2016).
- [24] H.-R. Wei, F.-H. Liu, and R. A. Lacey, J. Phys. G **43**, 125102 (2016).
- [25] S. S. Adler *et al.* (PHENIX Collaboration), Phys. Rev. Lett. **91**, 072301 (2003).
- [26] S. S. Adler *et al.* (PHENIX Collaboration), Phys. Rev. C **69**, 034909 (2004).
- [27] B. Alessandro *et al.* (ALICE Collaboration), J. Phys. G **32**, 1295 (2006).
- [28] B. Abelev *et al.* (ALICE Collaboration), Phys. Rev. C **88**, 044910 (2013).
- [29] E. Schnedermann and U. Heinz, Phys. Rev. C **47**, 1738 (1993).
- [30] L. Kumar (for the STAR Collaboration), Nucl. Phys. A **931**, 1114 (2014).
- [31] H. Zheng and L. L. Zhu, Adv. High Energy Phys. **2016**, 9632126 (2016).
- [32] J. Cleymans and D. Worku, Eur. Phys. J. A **48**, 160 (2012).
- [33] R. Odorico, Phys. Lett. B **118**, 151 (1982).
- [34] G. Arnison *et al.* (UA1 Collaboration), Phys. Lett. B **118**, 167 (1982).
- [35] M. Biyajima, T. Mizoguchi, and N. Suzuki, arXiv:1604.01264 [hep-ph] (2016).